journal of the international meteor organization

WGN

50:1
february 2022

ISSN 1016-3115

WGN Vol. 50, No. 1, February 2022, pp. 1 – 34

Administrative

Conferences

Radio Meteors

Ongoing Meteor Work

Front cover photo

This brilliant fireball was recorded on 2022 January 19 at $22^{h}34^{m}$ CET ($21^{h}34^{m}$ UT) from Soro, Denmark, using AllSky7 Camera System. The secondary dashed streak above the main fireball is an artifact. Photo courtesy: Henning Haack, `https://www.allsky7.net/`.

Writing for WGN

This Journal welcomes papers submitted for publication. All papers are reviewed for scientific content, and edited for English and style. Instructions for authors can be found in WGN **45:1**, 1–5, and at `http://www.imo.net/docs/writingforwgn.pdf` .

Legal address

International Meteor Organization, Jozef Mattheessensstraat 60, 2540 Hove, Belgium.

Janus

Cis Verbeeck[1]

As 2021 turns into 2022, there seems to be an atmosphere of cautious hope we can leave most of the restrictions and damage by the covid pandemic behind us. At the same time, the world is struck by a geopolitical disaster in Ukraine. In these difficult times, it's good to have hopes and wishes. First of all, I wish all our readers and their families a safe, healthy, prosperous, and rewarding year. I also hope we can meet again in person in 2022.

In 2021, Jean-Louis Rault and Rainer Arlt resigned as Director of the Radio and Visual Commission, and were replaced by Chris Steyaert and Jürgen Rendtel, respectively. Jean-Louis also left the IMO Council. In the 2021 IMO Council elections the President and all candidate Council members were elected for 2022–2025. We are happy to welcome new Council member Karl Antier, who is our webmaster since 2016. Juraj Tóth, Bob Lunsford, and Marc Gyssens fulfill specific responsibilities in the IMO Council, respectively as Vice-President, Secretary-General, and Treasurer. But several other people play an important role in IMO's activities. The IMO website, VMDB and fireball form are kindly provided and managed by Mike Hankey and Vincent Perlerin. Obviously, Javor Kac and his Editorial Board take care of producing a WGN issue every two months and have published IMC Proceedings articles for the IMC 2020 and 2021. The annual Meteor Shower Calendar, edited by Jürgen Rendtel, is one of the IMO's most successful products and reaches a large audience every year. Some work is less visible but not less important, e.g., Jan Verbert aids Marc Gyssens with the IMO finances, and Ronald Winkler takes care of the paper stock of IMO publications and ensures that WGN and IMC Proceedings articles make their way to NASA ADS in due time. The IMO news editors make sure that the IMO website stays up-to-date and reflects interesting meteor-related events or news, while the IMO info team answers questions posed to the IMO via e-mail. I am very grateful to all those people, and would like to thank them — and all people that I may have overlooked — for all the great work they have done and are doing for the IMO! It is also my pleasure to congratulate all persons with a recent new fole in the IMO, I wish them a lot of success and satisfaction in their new function!

Looking back on 2021, I believe we can say it was a year plenty of interesting events, with an unexpected Perseid outburst on August 14, some newly observed showers, and a predicted Aurigid outburst on August 31 – September 1. As always, several very bright fireballs were observed by camera networks and reported via the AMS/IMO online fireball form.

The year even saw the recovery of four meteorite falls: an iron meteorite weighing 14 kg in Sweden (associated with the November 7, 2020 fireball over Scandinavia), an L6 ordinary chondrite in Austria (associated with the November 9, 2020 fireball over Austria and neighboring countries), a meteorite fragment which smashed through a residential roof in British Columbia, Canada (associated with an October 3, 2021 fireball over British Columbia), and even the first carbonaceous chondrite fall ever recovered in the UK (associated with a very slow fireball over the UK on February 28, 2021).

Because of the pandemic, we had our second online IMC on September 25–26, 2021. The online IMC was a great success and reached more than 100 registered participants joining the IMC from different time zones (25 countries). Though, as probably most participants did, I really missed the extra benefits of an in-person conference, the IMC 2021 was very rewarding and I had the impression that most participants were better acquainted with the online character of the conference than in 2020. Going virtual also opened an opportunity for IMO to reach a new, wider audience, tearing down the financial and travel restrictions that refrain part of the meteor community to attend the regular IMCs.

In 2022, we are planning to organize an in-person IMC in Hungary on September 29 - October 2, in the small village of Poroszlo near Lake Tisza (Tisza-tó) in the Hortobágyi National Park. No, that is not entirely correct: we plan to organize a *hybrid* IMC, combining the benefits of an in-person conference with those of an online meeting. We are currently having final negotiations with the host site, and will report on the outcome soon via the IMO website and IMO News.

I hope to meet you face-to-face again, to share a drink, and to hear about your meteor activities in September. Meanwhile, have a great year!

Janus *was a Roman god with two faces, one looking to the past and one to the future, called upon at the beginning of any enterprise. Today he is often a symbol of re-appraisal at the start of the year.*

[1] Bogaertsheide 5, 2560 Kessel, Belgium.
Email: cis.verbeeck@gmail.com

IMO bibcode WGN-501-verbeeck-janus NASA-ADS bibcode 2022JIMO...50....1V

Letter — VLF signatures of meteors

George John Drobnock[1]

It is generally accepted that a meteor produces Very Low Frequency Signatures. There may be evidence that at higher frequencies meteors produce High Frequency (HF) or Very High Frequency (VHF) signatures (Obenberger et al., 2014). The meteor's tail does have sufficient ionization to reflect (scatter) HF and VHF electromagnetic signals (Opik, 1958). The hypothesis of this paper is that a meteor tail is a simple inductor and capacitor (LC) creating a tuned circuit that can resonate a specific frequency at any point during its flight. This resonance and observable frequency only occurs when $XL = XC$. Those who have observed for meteor signatures have reported that not all meteors produce VLF signatures. The possible explanation for not receiving a signature may be an inconsistency with the meteor having a resonance in relation to $XL = XC$.

Received 2021 October 16

1 Introduction

Since 1958, with the work of Hawkins (1958a,b), it has long been thought that a meteor creates an electromagnetic signature that can be rectified into an audible electrophonic sound, or that a meteor creates a receivable very low frequency wireless (radio) signal. In 1963 Romig and Lamar collected data on anomalous sounds and electromagnetic effects associated with fireball entry (Lamar & Romig, 1964). Keay, in 1980 pioneered initial research on anomalous sounds from the entry of meteor fireballs (Keay, 1980). Drobnock (1992, 2001, 2002) observed that meteors brighter than magnitude −6 produce an electromagnetic signature. In 1995 Beech, Brown, and Jones set out to detect and show that only meteors with magnitudes brighter than −6 would produce detectable vlf signatures. Price and Blum (2000) observed that during the 1999 Leonid Meteor Shower, meteors were producing electromagnetic signatures in both the ELF and VLF range.

Hawkins (1960) presented a paper on his work on electromagnetic emissions from meteors, in which he indicated that at the low end and the high end of the Very High Frequency spectrum there were no detectable emissions from meteors. Hawkins does state that during the observance of the 1959 Geminid shower there were some enhancements of low frequency magnetic noise.

On numerous occasions it was the sound, suggested to be an electrophonic noise, that caused the observer to look up. An obstacle immediately becomes clear: light from a meteor at an altitude of, say, 80 km (50 miles), would take only 0.0003 second to reach the ground-based observer whereas sound waves would take in excess of four minutes! Simultaneous observations of these two phenomena are not, apparently, possible. The solution to this problem may lie in the "hissing" sound that is often reported. Early radio (wireless) observers reported strong – stray – signals possible not sferics or atmospherics but meteors (Talman, 1922; Eccles & Airey, 1911).

Early wireless (radio) operators reported an occasional "rocket sound" or hiss. A report by W. C. Eccles (1911) discussing the recording of "Electrical Waves Occurring in Nature". His observation window as July 26 to August 31, 1910. It is interesting the period for the Perseid meteors is during these dates. He was doing his wireless experiments to identify "vagrant" signals that interfered with communications.

Havey H. Nininger (1952) in his classic book, "Out of the Sky", recalls that in 1934 E.R. Weaver of the US Bureau of Standards suggested that electromagnetic waves – or "ether waves" as Weaver called them – may be produced by meteors and fireballs. These would then be transformed into audible sound by objects such as buildings and cars.

Though ignored at the time, the proposal later received much attention, most notably by Colin S.L. Keay of the University of Newcastle in New South Wales, Australia. Keay has investigated reports of "electrophonic" sound emitted by a number of bright fireballs. In 1980 he showed that the plasma trail of a large fireball could generate Extra Low and Very Low Frequency (ELF/VLF) radio emissions in the range 1 to 10 kHz. His theory was eventually verified in 1988 by three groups of Japanese observers who, working together, managed to obtain simultaneous photographic and radio observations of a bright fireball together with an electrophonic sound report of the event.

Then there is also a controversy as to whether or not a meteor creates such an electromagnetic noise or signature. After years of radio observation, an electromagnetic signature has been heard on the lower end of the VHF radio spectrum. Although not always detecting a signature from a meteor, the meteor's trail will reflect a range of Earth bound transmitted signals.

Those observing a meteor or fireball for an electromagnetic signature have reported that not all meteors, even those that are anticipated to produce a signature (meteors with a magnitude brighter than −6) do have a detectable signature.

[1] Crum House, 213 South Jefferson Street, Mount Union, Pennsylvania. 17066 USA. Email: drobnock@penn.com

A meteor is to create an electrophonic sound from a nearby object, an object that has to resonate by the meteor's signature. The question then is, does a meteor act as a transmitter, producing a signature at a specific resonance?

2 Meteor Signature and Resonance

The possibility of a meteor creating an electromagnetic signature as discussed in the early days of wireless (radio) would have been created by a resonating circuit (Figure 1).

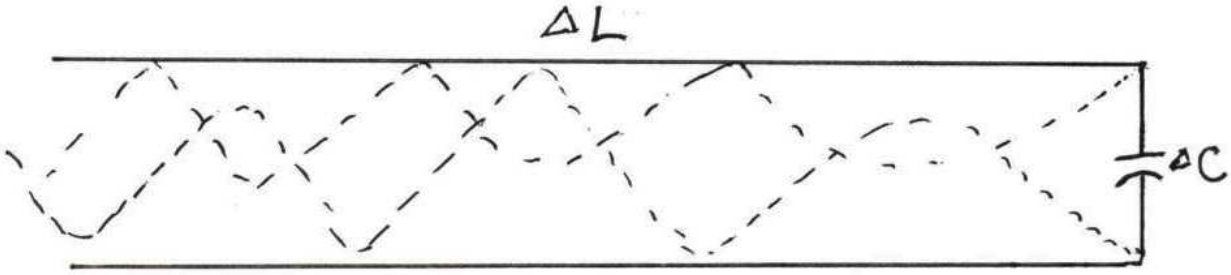

Figure 1 – A simple meteoroid resonating circuit can be illustrated as a natural capacitor and inductor of random inductance. As the capacitor and inductor can change in value until a random event causes the circuit to oscillate at a frequency determined randomly by the capacitor and inductor Where $XC = XL$.

For an electromagnetic signal to be created, a resonance mechanism needs to be available. Examples of uncomplicated oscillators (illustration the $XL = XC$ formula) are the discharges of a Leyden jar and Lecher wire with spark gap.

The resonance occurs by allowing an inductor XL and capacitor XC to be continuously charged and discharged to create a continuous wave. But with a meteor, the produced pulse or signature can be at a short time period (T). The result is a pulse at a frequency (f). The pulse responsible for a meteor's signature at a given frequency is created as the meteor travels into the atmosphere. The resonance can vary depending on the capacitance and inductance created by its aberration.

For a meteor to create a detectable electromagnetic signature, a resonating circuit needs to occur. This circuit needs to consist of a capacitor, an inductor, and resistance. The passage of the meteor through the atmosphere creates the energy to charge the circuit. A hypothetical model is shown in Figure 2. The twisting of the meteor's tail (Keay) creates capacitance. The length of the tail creates the inductor. The charge to the circuit is derived from the electrostatic charge created during the entry into the upper atmosphere. The capacitance and the inductor are constantly changing. At some random period during the flight the charge in the tail and the inductor resonate at a specific frequency (Carr, 1996; Rosenberg, 2005).

V.A. Bronshten suggests ELF/VLF radiation would be produced by trapping and tangling Earth's magnetic field in the turbulent plasma tail of an ablating meteoroid (Bronshten, 1991). This action would produce an ionized inductor. The possibility of ionized gas or plasma as an antenna or aerial was suggested by J. Hettinger in 1919.

For a circuit to resonate at a specific frequency, the resonance occurs by allowing an inductor XL and capacitor XC to be continuously charged and discharged to create a continuous wave. But with a meteor, a specific frequency is produced as pulse or signature that has a short time period (T). The pulse occurring may occur, all things being equal, only once. This signature is particular to the observed meteor. The result is a pulse at a frequency (f).

By definition resonance occurs when $XL = XC$, when $2\pi fL = \frac{1}{2}\pi fC$ (McHutchon, 2013):

$XL = (2\pi fL)$, where L equals inductance in Henrys and f equals frequency in cycles per second,

$XC = 1/(2\pi fC)$, where: C equals capacitance in Farads and f equals frequency in cycles per second.

Frequency is determined by the numbers of cycles of the electromagnetic signature at t in seconds.

$f = 1/T$ where f equals frequency in cycles per second, and T equals the period in seconds for a wave to resonate.

For a meteor to create an individual radio frequency signature please consider the following scenario:

1. The duration of the meteor's very low frequency electromagnetic signature pulse is short. It can start at less than 0.001 of a second. The pulse is of a short time duration and the resulting wavelength several thousand meters in length. A very long electromagnetic wave is produced; its range for reception is possibly a few hundred kilometers. However, this is not to say that a fireball magnitude of -6 or brighter will create a larger signature and its range may be greater, but in general the distance of a propagated signature from a meteor of magnitude -6 or less will be 300 kilometers or less. If the initial pulse from the meteor releases a signature for 0.001 seconds or less, the resulting signature will travel $d = r \cdot t$ (Figure 2).

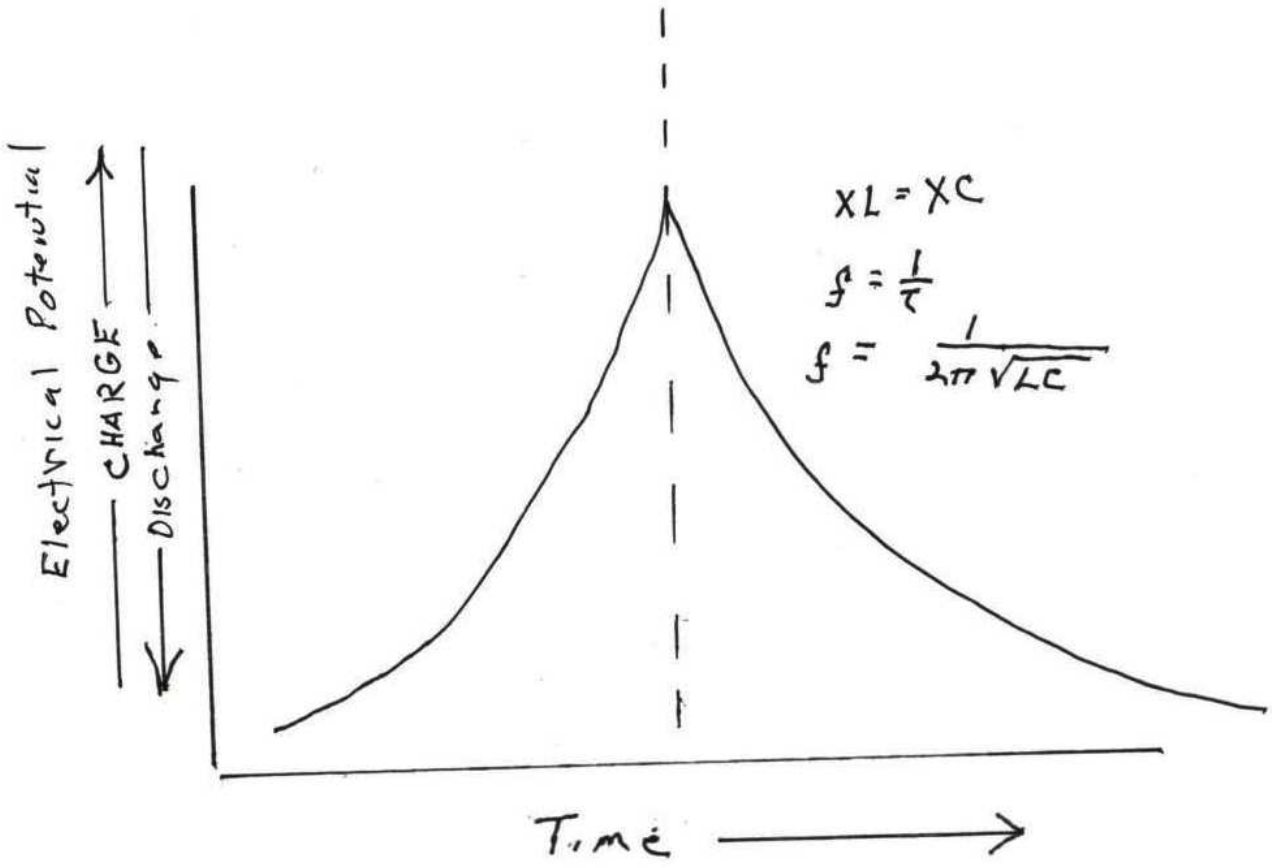

Figure 2 – During the meteoroids flight the values of the inductor (L) and capacitor (C) are constantly changing, whilst the internal capacitance is charging. At a random interval of time there is a discharge of the meteoroids natural capacitor, with the random value of the inductor produced by the twisting described.

Where d is the distance the pulse will travel, r is equal the speed of an electromagnetic wave in free space equals 2.9979×10^8 meters per second. The longer the pulse time T the greater the distance the signature will travel.

2. It is generally thought that a meteor "noise" is like to lightning generated sferics, creating multiple frequencies. If I may offer the following: Consider a meteor at its greatest ablation, before extinguish, and the release of the electromagnetic pulse as being a large resonating circuit. In order for an electromagnetic signature to be created there has to be resonance.

This is being modeled as a simple resonating circuit consisting of a capacitor and inductor. A simple tuned circuit that, when the energy is released from the capacitor, creates a single damper wave pulse.

3 The resonating circuit

The frequency generated by the meteor at the time of discharge of the electromagnetic pulse is dependent on the capacitance (in farads) created by the ablation of the minerals in the meteor and the upper atmosphere. This melting of silica, iron and low energy plasma of charged ions creates a temporary capacitor that is charged as it enters the atmosphere. The irons, siliceous materials, and plasma create the dielectric and electrode and charge of a temporary storage device. The length of the trail is plasma capable of acting an inductor. The length of the trail creates an antenna. The length of the trail would be an inductor measured in henries. The length of the resulting train or trail of the meteor and the capacitance created by a part the ablation of minerals would determine the frequency created.

The receiver used during the 2002 Leonids was tuned to 3 900 hertz. To generate a signature during the Leonids the meteor would have had to have an electrical discharge when the circuit was tuned with a resonating circuit having a capacitance of 0.002 microfarads and an inductor of 0.832 Henry. The length of the inductor or antenna would be 76.870 km. The capacitor created at some point reaches a breakdown point where the energy is released and resonance occurs in a given frequency of the VLF spectrum[a] – see Figure 3.

[a] https://goodcalculators.com/resonant-frequency-calculator/

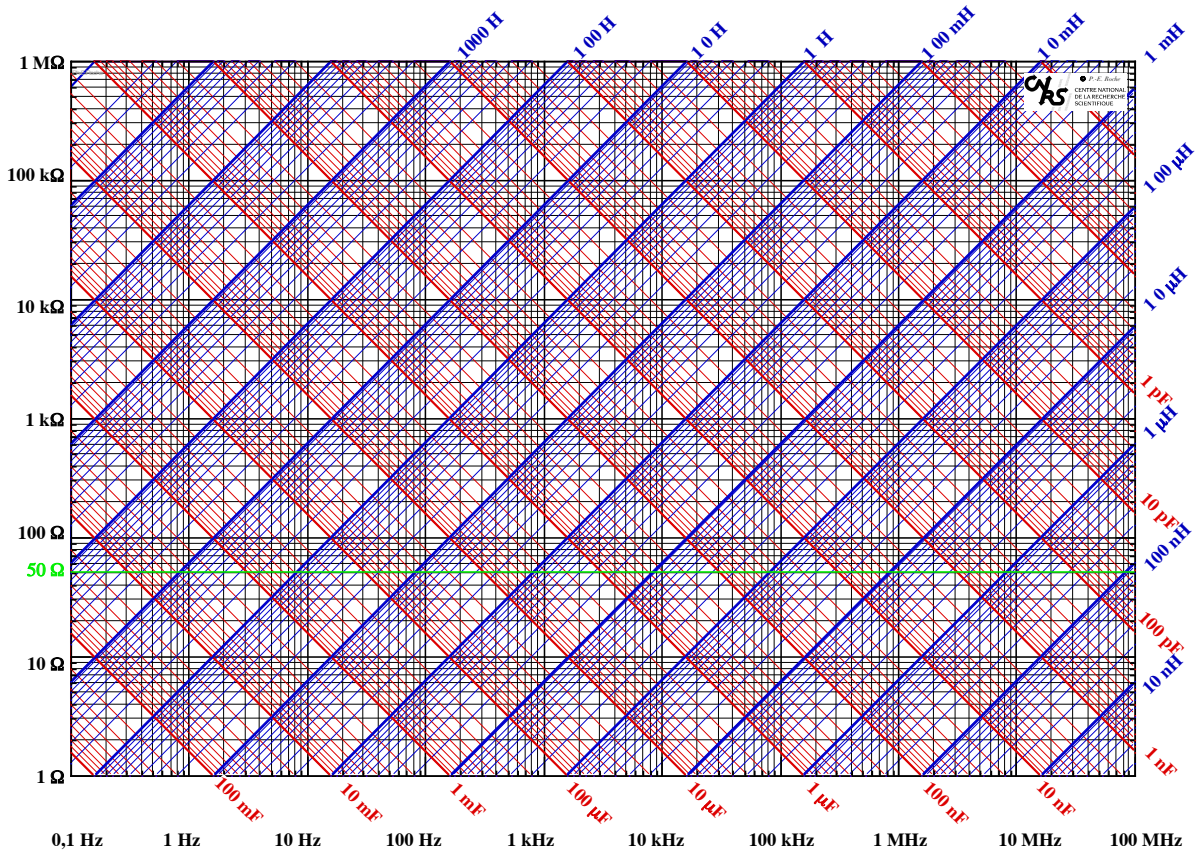

Figure 3 – Reactance Chart – The reactance chart is a document that allows the calculation of frequencies based on values of ohms, henries, and capacitance.

As the created signal is from an antenna in free space, the electromagnetic pulse has the probability of going off into space depending on the electron density of the atmosphere above and below the meteor, or around the meteor. The signature can be propagated to follow the curvature of the Earth, absorbed or attenuated by the atmosphere, and be "heard" in a different location (then it becomes a sferics). Or it can be propagated to the observer within a radius below the meteor's path.

4 Meteor as a Transmitter

Not every observation receives a signature from a single meteor. One explanation may be that the electromagnetic signal strength, in watts, may not correspond to the kinetic energy of a meteor. And given that the electromagnetic signature to the observer is subject to the inverse law for electromagnetic waves. The signature weakens the farther it travels from the source.

The meteor, as a transmitter, is constantly changing the length of the tail that acts as tuned inductor. The twisting of the tail can create the capacitance to store an electrical charge. The twisting is suggested by Beech and Bronshten, and Keay can create capacitance. The plasma antenna created and the capacitance is not constant through the entire flight. At the final stage of flight, when the electrical discharge occurs, the value of the inductor and capacitor (LC) is never the same and hence the frequency generated is never constant. Another factor to consider for the VLF signature to reach the observer is the standing wave created relevant to the length of the meteor's resonating circuit.

5 Signal Propagation

To support part of this please review reports of observations of the weak signal generated by Sputnik 1 (Kitchen, 1958).

The early satellite observations were on a weak continuous carrier wave, unlike a meteor generated pulse, but found to be subject to a varied propagation, unlike an Earth bound and generated signature. The early satellite observations were related to an orbiting transmitter of 100 watts at a frequency of 15 meters. The early observers noted that the satellite transmitter was transmitting in the D, E, and F layers of the upper atmosphere. The location of the transmitter in the upper atmosphere determined if the signal was received by an observer directly below the satellite or 1000's of kilometers away.

With a meteor's signature being of short duration and of varied energy it is possible to exhibit the same characteristics as the early orbiting satellite. But with a difference: rather than a continuous signal, the meteor signature is a short pulse that may or may not be observed.

The pulse, as with all electromagnetic energy, is subject to the inverse square law. As the signature radiates from its point of origin it weakens. A single pulse may not have enough energy to reach the observer. The distance an electromagnetic signature travels is related to distance is equal to the speed of the signature times the duration of the pulse, $D = R \cdot T$.

See attached diagram indicating some variables that my effect the character of a single meteor pulse signature.

This is not to say these are the frequencies of a meteor, but if the proposed meteor model of a natural capacitor and inductor created by ablation of a meteor when the trail reaches the length to resonate at say 3.9 kHz and there is a discharge of the natural capacitor, then a frequency is generated that is within the capability of my receiver.

The larger fireball may create additional signatures and have a sustained signature from its size, where the small meteor may create a signature for a very short time period. Therefore, limited period of the electromagnetic signature will make the success of capturing a meteor signal from a lesser fireball more difficult.

6 Conclusion

These notes are offering a possible model for a meteor creating a very low frequency electromagnetic signature. Observers using both meteor scatter and a VLF receiver have reported that a VLF signature is not always received, and there is a reported radio scatter. The creation of a receivable signature may be the interaction of the meteor creating a resonance in the electromagnetic spectrum.

References

Beech M., Brown P., and Jones J. (1995). "VLF Detection of Fireballs". *Earth Moon and Planets*, **68:1-3**, 181–188.

Bronshten V. A. (1991). "Electrical and Electromagnetic Phenomena Associated with Meteor Flight". *Solar System Research*, **25:2**, 93–104.

Carr J. J. (1996). *Secrets of RF Circuit Design, 2nd edition*. McGraw-Hill, New York, New York.

Drobnock G. J. (1992). "Radio Waves from a Meteor". *Sky and Telescope*, **83**, 329–330.

Drobnock G. J. (2001). "Meteors Producing VLF Signatures Independent of Producing Electrophonic Sounds". *WGN, Journal of the IMO*, **29:1/2**, 45–50.

Drobnock G. J. (2002). "VFL Signatures from non-fireball meteors – Observations from the 2001 Leonid shower". *WGN, Journal of the IMO*, **30:5**, 152–156.

Eccles W. H. and Airey H. M. (1911). "Note on the Electrical Waves Occurring in Nature". *Proceedings of the Royal Society of London Series A*, **85:576**, 145–150.

Hawkins G. S. (1958a). "A Search for Radio Emission from Meteors.". *Astrophysical Journal*, **128**, 724.

Hawkins G. S. (1958b). "Radio Noise from Meteors". *Nature*, **181:4623**, 1610.

Hawkins G. S. (1960). "Electromagnetic emission from meteors". In Menzel D. H., editor, *The radio noise spectrum*, pages 79–92. Harvard Univ. Press, Cambridge, Mass.

Keay C. S. L. (1980). "Anomalous Sounds from the Entry of Meteor Fireballs". *Science*, **210:4465**, 11–15.

Kitchen F. A. (1958). "Direction-finding observations on the 20 MHz transmissions from the artificial Earth satellites". *Proceedings of the Royal Society of London. Series A, Mathematical and Physical Sciences*, **248:1252**, 63–68. (Oct. 28, 1958).

Lamar D. L. and Romig M. F. (1964). "Anomalous Sounds and Electromagnetic Effects Associated with Fireball Entry". *Meteoritics*, **2:2**, 127.

McHutchon A. (2013). "Rlc resonant circuits". `https://mlg.eng.cam.ac.uk/mchutchon/ResonantCircuits.pdf` .

Nininger H. H. (1958). *Out of the sky: An introduction to meteoritics*. Dover Publications, Inc.

Obenberger K. S., Taylor G. B., Hartman J. M., Dowell J., Ellingson S. W., Helmboldt J. F., Henning P. A., Kavic M., Schinzel F. K., Simonetti J. H., Stovall K., and Wilson T. L. (2014). "Detection of Radio Emission from Fireballs". *The Astrophysical Journal Letters*, **788:2**, L26.

Opik E. J. (1958). *Physics of meteor flight in the atmosphere.* Interscience Publishers.

Price C. and Blum M. (2000). "ELF/VLF Radiation Produced by the 1999 Leonid Meteors". *Earth Moon and Planets*, **82-83**, 545–554.

Rosenberg P. (2005). *Basic Electronics.* Wiley Publishing, Inc., New York, New York.

Talman C. F. (1922). *Meteorology: The Science of the Atmosphere.* Vol 1. of the Popular Science Library. P. F. Collier.

IMO bibcode WGN-501-drobnock-letter NASA-ADS bibcode 2022JIMO...50....2D

Editorial note: Some of the statements in this letter are very speculative.

Conferences

Forty-First International Meteor Conference, Poroszló, Hungary, 2022 September 29 – October 2

Ákos Kereszturi [1]

1 Introduction

The conditions for the organization of the annual International Meteor Conference are still not normal, however current regulations because of the COVID-19 virus allow the organization of physical meetings. Thus the IMO Council and the Hungarian organizers progress with the preparations and hope the conditions will remain the same as now and allow the meeting to take place. The organizers encourage you to register, as the site can accommodate 120 people on a first come first served basis. In case the meeting cannot be organized, full registration fees will be reimbursed to the registered persons.

Most of the scientific analysis based forecasts of experts suggest that the virus and the related uncomfortable situation will not disappear for about a year, and persons interested in international conferences could meet with each other if restrictions are kept carefully. The IMC 2022 provides all obligatory and recommended restrictions to keep a safe meeting. The conference site is accessible by cars from European countries without flight, all facilities support hygienic presence of attendees at this remote, countryside location. The Local Organizing Committee is composed of members from the Konkoly Astronomical Institute (Research Centre for Astronomy and Earth Sciences).

2 Venue and location

The conference site is at the Great Hungarian Plain, Hortobágy area, nearby a village called Poroszló, about 140 km to the east of Budapest, 2 hours driving distance (Coordinates: 47.649976° N, 20.668603° E; Google maps link at `https://tinyurl.com/IMC2020-map`), at the lake called Tisza-tó, at the area of the Natural Reserve Hortobágy (part of the UNESCO World Heritage sites). The "Fűzfa Hotel és Pihenőpark" (Willow Hotel and

[1] Research Center for Astronomy and Earth Sciences. E-mail: `kereszturiakos@gmail.com`

Figure 1 – Location of the site on a map (left) and its aerial view (right).

Figure 2 – Images of the main building (top left), one room interior (top right), some of the wooden houses (bottom left) and their interior (bottom right).

Recreation Park, `https://fuzfapihenopark.hu/`) is a farm-like hotel, with buildings in 100–200 m walking distance from each other.

While the conference room can host 120 persons, there are only 95 beds on-site, 8 of which are available in single rooms, at a single room surcharge. Half of the on-site beds are in a large house as separate rooms with 2, 3 and 4 beds, while the remaining half of the beds are located in small wooden houses. All rooms are equipped with private bathroom, fridge, air conditioning, and WIFI access. In case all the 95 beds are reserved, further applicants can reserve a room for themselves in nearby accommodation and pay only the non-accommodation registration fee (including conference costs and meals but not accommodation). The organizers will suggest alternative accommodation in the village.

The site includes thermal bath, sauna, indoor swimming pool and outdoor thermal bath, which could be used free of charge during the conference (Figure 3). There is a "night bar" where various drinks could be bought (only for national currency called forints and not Euros), three billiard tables can be used next to chairs and tables, around three bowling alleys (this last is not free of charge for use and the drinks in the bar should also be paid for).

Figure 3 – The bowling alleys (left), the indoor swimming pool (middle) and the outdoor thermal bath (right).

The weather at the end of September is supposed to be mild with max. 20–25°C temperature daytime, 10–15°C nighttime and low probability of rain. Mosquitoes might be present, thus you might want to bring some spray against mosquitoes. In case you require a visa, please contact the local organizers as soon as possible. The local currency of Hungary is forint (HUF) – Euro is not accepted. You need to convert your currency, which should be done in the main cities, however you may use your credit card.

3 Program and events

The scientific program will start in the evening of Thursday September 29 and will terminate at lunch Sunday October 2. The excursion of the IMC 2022 will happen in the afternoon of Saturday October 1. The location is the natural reserve next to the meeting place, part of the Hortobágy National Park. The excursion will contain two parts, participants will be divided in at least two groups, with alternating site visit, altogether for 2–3 hours:

1. The walking along the "water pathway" that follows a 1.5 km long wooden plank system above the water, meandering in the reed system. The pathway crosses 3 small islands, 2 bird watching hides and a 15 m high scene watching tower. Information tables and guides will help you to get familiar with the unique plants and animals there.

2. The boat trip also takes you through the natural reserve, visiting such hidden locations that are not accessible during the walk. The natural environment is almost intact at the excursion site, thus please follow the directions and the rules explained by the guides, and consider the environment, keeping your trash with you and bringing it back to the hotel.

4 Travel info

The conference site can be reached by a 2 hour drive from Budapest. For persons arriving at the airport, a shuttle service will be provided if needed. You can indicate your request to use the shuttle in the registration form. The shuttle costs 45 EUR per person. For an ideal organization, please give your flight number and arriving / departing times as well.

Figure 4 – The "water pathway" part of the excursion.

- Flight: to Budapest (BUD) Liszt Ferenc International Airport. From there the local organizers arrange 2 shuttle services around noon and late afternoon of the first day. There is a train access possibility from Budapest to Poroszló (see below).
- Car: this is the ideal method to come to the site, which requires 2 hours driving from Budapest (mainly on the M3 highway that requires a highway access ticket that costs 12 EUR). The travel time from some main cities by car are the following: Bratislava 3.5 hours, Prague 7 hours, Berlin 12 hours.
- Train: from Keleti pályaudvar, i.e. the East railway station trains run around every 3 hours, the trip takes around 3 hours, but requires 3 changes (usually at Hatvan and Fuzesabony). For more information ask the LOC.

5 Registration and payment

The registration for the meeting will soon be opened at `https://imc2022.imo.net/registration`. The early bird registration fee (until June 30) is 225 EUR for standard accommodation in all room types excluding single rooms for 3 nights with full board + participation in the conference, conference materials, coffee breaks and excursion (price per person). There is a limited availability for single rooms (350 EUR, maximum 8 rooms), which covers the accommodation in a single room for 3 nights with full board + participation in the conference, conference materials, coffee breaks and excursion. There is a possibility to pay 100 EUR with no accommodation but with all meals except breakfasts + participation in the conference, conference materials, coffee breaks and excursion (for people who book accommodation off-site). After June 30, 20 EUR will be added to all registration fees. It is also possible to attend the conference online (0 EUR). For more details, please visit the IMC 2022 website at `https://imc2022.imo.net`. We hope to finally meet you again at the IMC in Hungary!

COVID-19 Info

We hope that the IMC 2022 in Hungary can take place as planned, on September 29 – October 2, though this of course depends on the evolution of the COVID-19 pandemic and related policies. Please bring your vaccination certificate with you.

We encourage people to register for the conference. The following guarantees may be of help:

1. In case the IMC 2022 is canceled due to COVID-19, all participants will get a total refund.
2. If travel between a participant's country and Hungary is not allowed at the time of the IMC, the participant will get a total refund.

Radio Meteors

The Randomness of Sporadic Meteoroids in Radio Observations

Hans W. Wilschut[1] *and Felix Verbelen*

We examine an uninterrupted set of radio observations of mostly sporadic meteoroids to determine whether these meteoroid events occur purely randomly in time or whether short burst of events may contribute. Event clustering on a short time scale of about a minute, but larger then one second, is examined in a background of statistically distributed events modulated with a diurnal dependence. We find that in the present data set all events can be attributed to chance coincidences. It is also shown that if some occasional clustering does occur, this can not be identified by statistical means based on event timing only, thus requiring additional observables.

Received 2022 February 13; in original form 2021 September 14

1 Introduction

When observing radio echos from forward scattering a range of phenomena are found, such as Doppler shifts, Fresnel oscillations, or head echos. By recording only the time of such events with a time resolution of about a second one gets a good impression of the meteoroid activity, for example to study meteor showers. One may wonder if there is more information in these data streams. When reviewing series of meteor radio reflections, compact groups of events quite often seem to appear. Since these reflections are mostly separated by intervals of several seconds, they cannot be meteors disintegrating during their brief passage through the Earth's atmosphere. They could however be correlated particles split-off recently from a larger parent fragment. The degree of time clustering could then be an indication how recently such an event occurred. In general, meteoroids are observed to occur randomly in time apart from an overall slow variation, in particular, the diurnal and annual dependencies. To find whether a data stream is purely random on a certain time scale (to be defined later) or if it contains events clustered in time, a statistical analysis is required.

In this paper we will show explicitly that sporadic meteoroids at a timescale larger than a second occur predominantly in a stochastic time sequence described by statistical theory. Within these events we then investigate whether clusters can be identified.

As basis for the current investigation the registrations of radio meteoroids obtained during the second half of January 2021 at Kampenhout (BE) at the frequency (49.99 MHz) of the VVS beacon at Ieper (BE) (Steyaert, 2006) were used. The data are collected by an automated system all with the same setting and thus have been measured with a common bias. For the present investigation a period in January was chosen when few meteor showers were active and the events are therefore dominated by sporadic meteors and the event rate is most uniform except for the diurnal variation. The data are a relatively small time-range selection of about 400 hours from a much larger body of data that are regularly[a] published in e.g. Meteor News.

The outline of this article is as follows. In section 2 we discuss the diurnal variation of radio meteors. This is needed to obtain a value for the average event rate in a certain time range, which is an important input for testing the hypothesis of short burst occurrences. In section 3 we discuss the statistical theory describing random events occurring with a constant average event rate. In particular, we derive the chance to see a number of events in a particular time window. In this section we also introduce a convenient Monte Carlo method for data simulation. The statistical analysis of the observational data is made in section 4. We find satisfactory agreement with a stochastic distribution of the event data. In section 5 we investigate how a component of non-statistical event distributions could be found by adding and subsequently recovering a random burst to, respectively from, the data. In the concluding section 6 we summarize and discuss shortly how the current result can be used to examine fragmentation of meteoroids on a time scale shorter than a second.

2 Diurnal variation

The observed meteoroid event rate, λ, shows a strong variation with the time of day (McKinley, 1961). For our analysis we will need a prediction of the event rate that is better than just averaging the event rate over an hour. Therefore, we try to find a phenomenological description of the average number of events per hour. The data points shown in Figure 1 are the observed number of events per hour. The daily (diurnal) variation is clearly visible in the figure. Indicated is also the uncertainty in these numbers, which is taken to be their square root. Note, that this already assumes that the number of events in an hour follow a Poisson distribution, i.e. that events are randomly distributed. We tried two different approaches. The first one assumes a sinusoidal dependence with a frequency of 24 hour, to which an overall slow variation is added by trial and

[1]van Swinderen Institute, University of Groningen.
Email: hwwilschut@gmail.com;
permanent address: Sankt Augustin, Germany.

IMO bibcode WGN-501-wilschut-randomness
NASA-ADS bibcode 2022JIMO...50...12W

[a]Felix Verbelen's monthly radio meteors reports at https://www.meteornews.net. The data with one second resolution in this article are available as https://www.vvs.be/system/files/20210115-20210131_49990_fv_all.txt

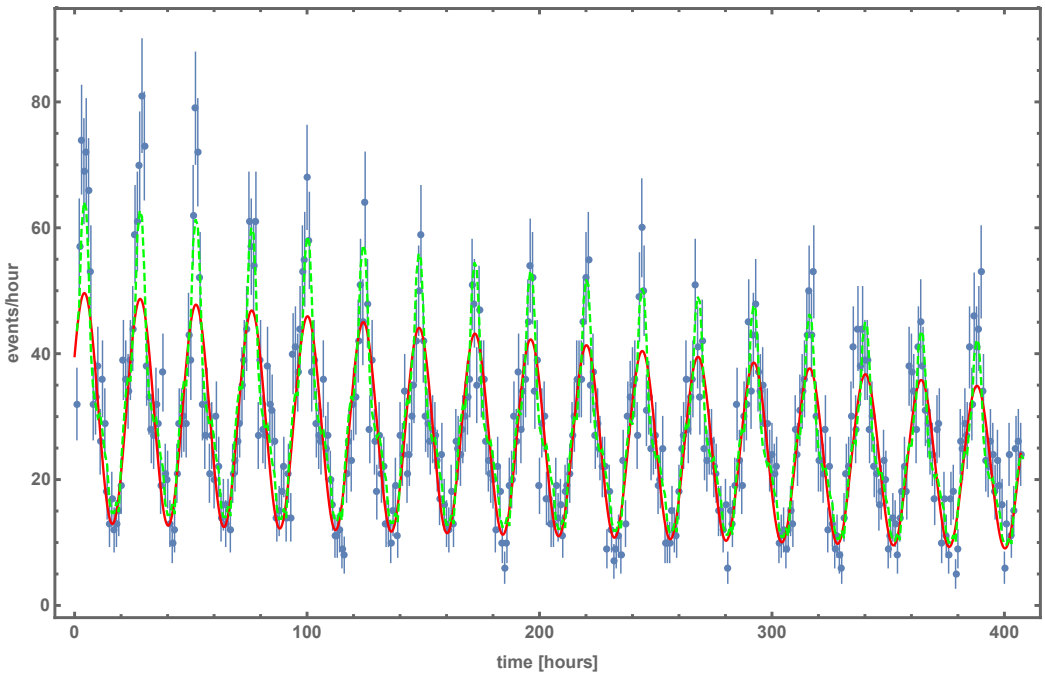

Figure 1 – [Color on-line] The number of observed event rates in bins of one hour (blue points). The statistical error bars are indicated. The red curve assumes a sinusoidal diurnal dependence, while the dashed green curve assumes that the event rate has each solar day the same time dependence, only the overall scale is varying. See text for more detail.

error. A reasonable description of λ is found as

$$\lambda(t) = a + bt + c(1 + dt)\sin(\frac{2\pi}{24}t + \phi), \qquad (1)$$

where the parameters $a..d$ describe the slow overall variation and ϕ is the diurnal phase. It is displayed as the red curve. The least-square fitting procedure for the about 400 points in Figure 1 gives a reduced χ^2 of 1.7.

The second approach assumes that the shape of the distribution is each day identical, only the overall scale changes. The shape, $S(t)$, is obtained by averaging over all available days. We use

$$\lambda(t) = (a' + b'(t \div 24) + c'(t \div 24)^2)S(t \bmod 24). \quad (2)$$

Again the parameters $a'..c'$, describe a slow variation over the course of the whole measurement. The count rate function is shown as the green dashed curve. In this case the reduced χ^2 is 1.2, where we note that $S(t)$ is constructed from the observational data, so that the reduced χ^2 is non-trivial. Both fits do fail the χ^2 test by far (the best P-value is 0.3%), which is associated with the large number of data points relative to the simple description with few parameters. However, for the purpose of the following analysis they suffice. As the second method gives the best parameterized dependence for $\lambda(t)$ we will use it in the following. It was checked that our results did not depend on the detail of the diurnal description.

3 Statistical theory

The chance an event occurs starting a time $t = 0$ is given by the exponential distribution (Particle Data Group et al., 2020)[b]

$$P_1(t) = \lambda e^{-\lambda t}, \qquad (3)$$

where λ is the average event rate and t the time elapsed for the event to occur. Waiting a time t after a previous event, the meaning of t becomes the waiting time between consecutive events. The highest probability is, largest for $t = 0$, but the average waiting time remains, of course, the inverse count rate:

$$\int_0^\infty \lambda t e^{-\lambda t} dt = \frac{1}{\lambda}. \qquad (4)$$

Another result of statistical theory generalizes Equation (3) and gives the distribution of waiting times for the last of n events to occur given a starting point (Particle Data Group et al., 2020)[a].

$$P_n(t) = t^{n-1}\lambda^n e^{-\lambda t}\frac{1}{(n-1)!}. \qquad (5)$$

To conclude this technical section we introduce a convenient Monte Carlo technique for producing a sequence of events randomly in time. We use the inverse transform method (Particle Data Group et al., 2020)[c] Integral of Equation (3) between 0 and t_r, corresponds with a random numbers, rnd, between 0 and 1, from which t_r follows

$$1 - e^{-\lambda t_r} = rnd \rightarrow t_r = \frac{1}{\lambda}\ln(\frac{1}{1-rnd}) \equiv -\frac{\ln(rnd)}{\lambda}. \qquad (6)$$

Note that $1 - rnd$ is also a random number, therefore the last two expression are equivalent. We illustrate the theory above by producing a sequence of events similar in length and count rate as in the observation, but with a constant rate of 36 events/hour (i.e. $1/\lambda = 100$ s). The event times t_i are simply obtained by

$$t_i = t_{i-1} + t_{ri}. \qquad (7)$$

[b] https://pdg.lbl.gov/2020/reviews/rpp2020-rev-probability.pdf

[c] https://pdg.lbl.gov/2020/reviews/rpp2020-rev-monte-carlo-techniques.pdf

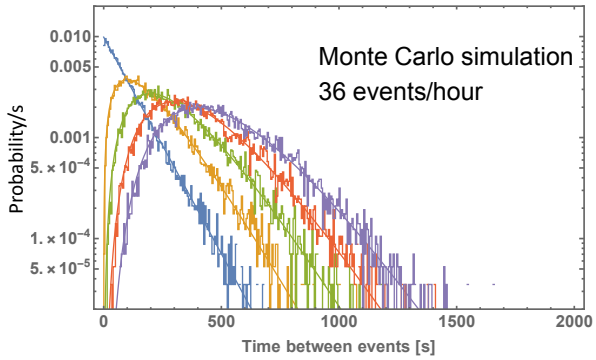

Figure 2 – [Color on-line] Data from a Monte Carlo event generator assuming on average 100 seconds between events corresponding to a rate of $\lambda = 36$ events/hour. Curves through the histogrammed data are theoretical descriptions with $n = 1..5$, they are explained in the text. The straight blue line through the corresponding data is the probability distributions for waiting times between events ($n = 1$). The orange curve is the distribution of times starting with a certain event and waiting until two events have occurred ($n = 2$). Green, red and purple, corresponds similarly to distributions for $n = 3, 4$ and 5, respectively. Note the logarithmic vertical axis.

.

Of course, for each new element i in the event stream a fresh random number needs to be drawn for t_{ri}. The waiting time t for n subsequent events, i.e. $t = t_{i+n} - t_i$, are put in histograms with a convenient bin width. After filling the histogram we normalize them to obtain probability density functions (PDF's) that can be directly compared with the theoretical expressions. These normalized histograms are referred to as the observed waiting time distributions, $P_n^{obs}(t)$. In Figure 2 these distributions are shown together with the theoretical functions $P_n(t)$.

The histograms and theoretical functions agree very well (by construction). Note that the maximal probabilities are at $t = (n-1)/\lambda$.

4 Statistical distribution of meteoroid events

We apply the procedure discussed in the previous section to the observed data stream. The event rate is determined for each $P_n^{obs}(t)$ separately by a fit to the corresponding data which have been histogrammed in the way described in the previous section. The results are shown in Figure 3.

The fitted values $1/\lambda = 107.7 \pm 0.7$ are consistent with each other. The value obtained from the data rate averaged over the full data set is however 127.5 s. The fitted $P_n(t)$ described the data poorly and less so as n increases.

The lack of agreement between theory and data in Figure 4 is due to the diurnal variation. This needs to be included in the theoretical description in someway. We choose to do this by creating simulated data where we track the hourly event rate. This is done by making an event series

$$t_i = t_{i-1} + \frac{-\ln(rnd)}{<\lambda>_{t_i}}. \qquad (8)$$

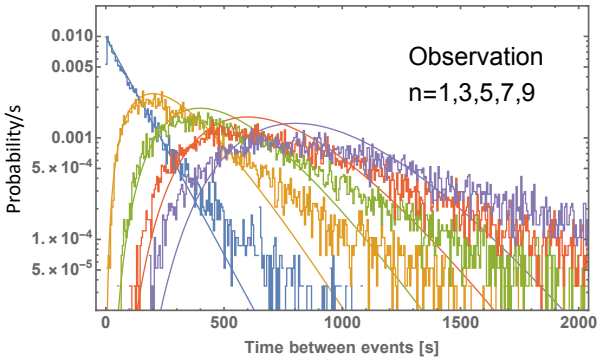

Figure 3 – [Color on-line] As in Figure 2 using the measured data. For clarity we show only $P_n^{obs}(t)$ with $n = 1, 3, 5, 7$ and 9.

.

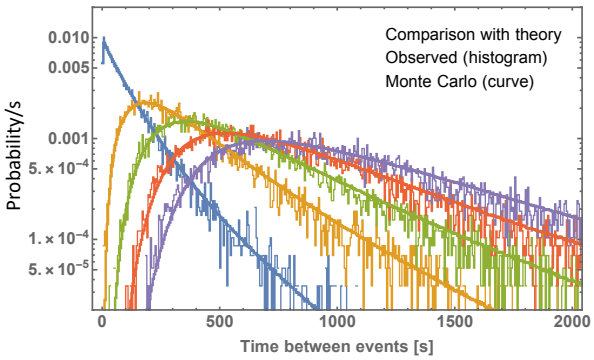

Figure 4 – [Color on-line] Comparison of the observational data, $P_n^{obs}(t)$ with $n = 1, 3, 5, 7$ and 9 with the corresponding Monte Carlo simulation using a local time average of the data rate.

.

Here $<\lambda>_{t_i}$ is a local time average rate, as described in section 2. We use the rate function based on the diurnal repetition Equation (2) These data are then used to obtain the Monte Carlo version of $P_n^{obs}(t)$. To remove the statistical fluctuation we repeat the procedure 1000 times and take the average, this eliminates the fluctuations in the calculated probabilities. We will refer to these distribution functions as $P_n^{MC}(t)$ in the following. They are the equivalents of Equation (5). The comparison is shown in Figure 4. Here the histogram representing the theory, i.e. $P_n^{MC}(t)$, appears as a smooth line due the averaging procedure. Now, a much better agreement is found than in Figure 3. Note that the theory is not fitted to the data, the only parameter, λ, is the event rate, which is obtained with the procedure in section 2.

One feature in Figure 4 should be noted. The drop in the first bin of $P_1^{obs}(t)$ (bin widths are 5 s), is a dead time effect. In the observations events need to be separated by at least a second in order to see them as separate events. Moreover strong signals (overdamped events) may obscure following weaker events. In the Monte Carlo simulations we required a minimal separation of 2 s between events to get agreement with the data.

Clearly one may conclude that the event stream consists of locally stochastically distributed events. By taking the modeled slowly varying meteoroid rate as the

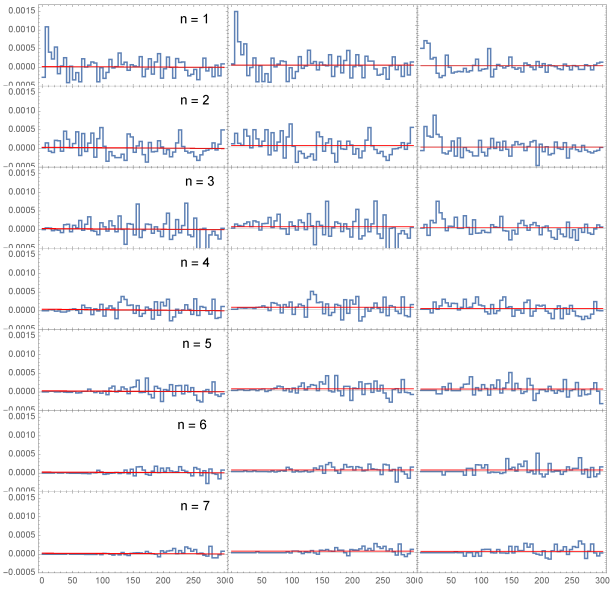

Figure 5 – [Color on-line] Left column:$P_n^{obs} - P_n^{MC}$, Middle column: $P_n^{obs+b} - P_n^{MC}$. Right column $P_n^{obs+b} - P_n^{obs}$. The vertical scales ranges between -5×10^{-4} and 15×10^{-4}/bin of 5 seconds. In the right column the vertical scale has been enlarged by a factor 5. The horizontal scales are between 0 and 300 s. Further details are in the text.

.

count rate, one has taken this non-statistical variation into account. However, the question remains whether there is room for non-statistical events like short bursts of data.

5 Search for non-statistical time distribution of meteoroid events

To find if the data stream could contain events that are of non-statistical origin, e.g. a sudden bursts of data due to clustering, we inject into the observational data deliberately random bursts of events which we would then need to find back in the analysis. Here, we put 20 bursts at random times in the data event stream. Each burst consists of 4 radio signals that are taken at random from a normal distribution (Gaussian) with a standard deviation of 10 seconds. The modified event stream is then analyzed as before. The probability distributions are evaluated and assigned to $P_n^{obs+b}(t)$. The label $obs+b$ refers thus to the actual observations spiked with the artificial bursts.

The probability distributions found this way are barely different from those of the original data. In Figure 5 this is shown. First we subtract the Monte Carlo probability $P_n^{MC}(t)$ from the true probability distribution $P_n^{obs}(t)$ (the curve and data shown in Figure 4). This difference is shown in the left column of plots labeled with n. We show the same in the middle column for the difference between the observed data spiked with the 20 burst and the Monte Carlo result. (The Monte Carlo was recalculated to account for the change in $\lambda(t)$ due to the added 80 events.) The data in the two columns are very similar indicating that the effect of the 20 bursts is nearly negligible. To see what, in fact,

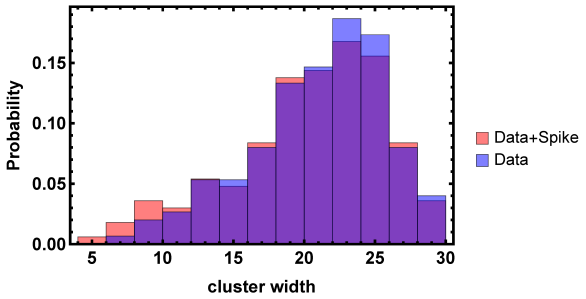

Figure 6 – [Color on-line] The width distribution (normalized to unity) of clusters shorter than 60 s for the event data and the data spiked with sharp clusters. (Overlapping bars mix colors to a darker hue.)

the contribution is, we subtract the observed probability distributions from the spiked ones, to isolate the effect of the spiking. This is shown in the plots of the right column where we multiplied the probabilities with a factor 5 to make the result visible. A small enhancement is seen at small times for the probabilities with $n \leq 3$, consistent with 4 neighboring events. (The first event is the beginning of the cluster, the last event ($n = 3$) the end.) Although we retrieve the effect of the spiked events, the procedure is not very promising to search for non-statistical events in an actual data stream.

An alternative approach is to search explicitly for clusters. To explore this option we require that at least 4 events ($n \geq 3$) occur within 60 seconds. In addition to the about 150 cluster in the original data, the algorithm employed[d] finds back all 20 spiked events described above, some of them include an event of the actual data. A convenient way to look at this, is by evaluating the distribution of the width, σ, of the clusters, i.e. $\sigma = \sqrt{\sum_{i \in \text{cluster}} (t_i - <t>_{\text{cluster}})^2 / n}$, with $<t>_{\text{cluster}}$ the mean time of the cluster. The spiked events have σ distributed around 10 by their construction. The cluster-width distribution is shown in Figure 6. Enhancement around $\sigma \approx 10$ is clearly seen when compared to the distribution without the spike events. Note that, because the distributions are normalized to unity, the maximum at $\sigma \approx 25$ of the spiked distribution is also lower than the original one. This methods of finding clusters thus works if a sufficiently strong component of events with similar characteristics occur in the data.

Comparing the width distributions of the event data with those of the simulated event data (Figure 7) we observe no clear difference. From which one can conclude as before that there is no clear sign of short-burst clusters. Any clustering will be hidden in the statistical fluctuations of the distributions.

6 Conclusions and Outlook

When one takes slow changes in the sporadic meteoroid count rate into account, the radio events are occurring randomly in time. This is shown in this work by a detailed comparison of the event distribution with

[d]The function "Gather" in Wolfram Mathematica.

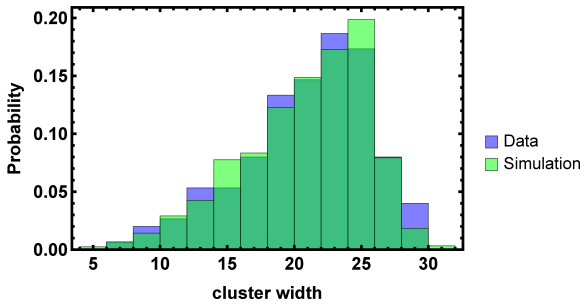

Figure 7 – [Color on-line] The width distribution (normalized to unity) of clusters shorter than 60 s for the event data and the simulated event data.

those generated in a Monte Carlo simulation with random events. The second result of the present study shows that short bursts of clusters will, in general, not be recognized as they can not be distinguished from the statistical event stream. Only if they occur with similar characteristics and sufficient frequency can they be identified.

The results of this work may be fruitful for the analysis of data taken with a higher time resolution. Here the meteoroid class with a head echo can be used to characterize the radio events further using the Doppler shift information. In this case fragmentation in the atmosphere will show up as clusters in a time region of at most a few seconds. The present analysis shows how to determine in that case the background of clusters occurring by chance on basis of the average event rate. Additional information may also help to give a better characterization of clusters hiding in the statistical background.

Acknowledgement

One of the authors (H.W.) thanks C.J.G. Onderwater for reminding him of the "how to do it" reviews of the Particle Data Group (Particle Data Group et al., 2020).

References

McKinley D. (1961). *Meteor Science and Engineering*. McGraw-Hill, New York.

Particle Data Group, Zyla P. A., Barnett R. M., Beringer J., Dahl O., Dwyer D. A., Groom D. E., Lin C. J., Lugovsky K. S., Pianori E., and et al. (2020). "Review of Particle Physics". *Progress of Theoretical and Experimental Physics*, **2020:8**, 083C01.

Steyaert C. (2006). "The VVS meteor beacon". In Bastiaens L., Verbert J., Wislez J.-M., and Verbeeck C., editors, *Proceedings of the International Meteor Conference, Oostmalle, Belgium, 15-18 September, 2005*. pages 25–33.

Handling Editor: Javor Kac
This paper has been typeset from a LaTeX file prepared by the authors.

Ongoing Meteor Work

Ablation & Fragmentation Model (AFM): a simple phenomenological simulation of meteoroid ablation and fragmentation

J. Vaubaillon[1], *R. Decosta*[2], *D. Hestroffer*[2]

Many celestial objects – of different sizes – are evolving in the Earth's space environment, so that approximately 30000 tons of extra-terrestrial material enters the Earth's atmosphere every year, some of them reaching its surface. The size of these objects, from micro-meter sized dust – yielding shooting star meteors, to larger 0.01 to 1 kilometer – with higher impacting consequence and hazard, have different frequencies of associated events. Understanding and modeling the interaction with the atmosphere is of importance to rapidly assess their potential risk, or to find the meteoritic remnants that are precious cosmic "sample returns". The risk (that is probability and consequence of an event) and hence protection or mitigation of Earth's atmosphere is probably larger for meter to 100 m sized bodies that can reach low altitudes, produce meteorites, shock waves or even impacting craters. In order to predict the possibility that an entering bolide can produce a meteorite and find in short-term its subsequent location on the ground, we have developed the "AFM" (Ablation and Fragmentation of Meteoroids) tool to model two principal phenomena appearing during a hypervelocity atmosphere entry: *ablation* and *fragmentation*. "AFM" is a software written in Fortran 90 that simulates such phenomena according to a chosen model. The AFM tool does not include high HPC computation with full hypervelocity hydro-dynamics model, but it is simple and robust in order to provide good and reliable first order approximation of the atmospheric entry and final outcome of meteorites on the ground. We present here the atmosphere model used and the physical modeling implemented to predict sizes and number of particles of a given size as function of the altitude. Application can be on prediction of meteorites reaching the Earth, or particles at about 10 km that could present risks to civilian aviation.

Received 2021 December 3

1 Introduction

Thanks to the spread of meteor camera networks (Spurný et al., 2007; SonotaCo, 2009; Jenniskens et al., 2011; Bland et al., 2012; Srba et al., 2016; Wiśniewski et al., 2017; Segon et al., 2018; Colas et al., 2020), to mention the most recent, the search and successful recovery of meteorite following a recorded fireball has greatly increased. Such fireball sometimes exhibits flickering or fragmentation (Pearson et al., 2005; Popova et al., 2011; Borovička et al., 2013). When searching for meteorite, the knowledge of what to look for is better. The main question is to know the mass (or size) of the main fragment, and the existence of smaller fragments and subsequent spread on the ground. For this and to better understand the meteor phenomenon, the determination of the initial mass of the meteoroid, or the terminal mass of the main fragment has been the topic of several studies (see e.g. Moreno-Ibáñez et al., 2015; Sansom et al., 2019). In addition, in order to better derive the entry speed and thus also the orbit of the meteoroid, atmospheric deceleration must be properly described. Optical observation may be coupled with a model of disintegration and possible fragmentation (Campbell-Brown et al., 2013; Vida et al., 2021). Knowing that even the smallest meteoroids do fragment, this process is of utmost importance to understand the meteor phenomenon (Armitage & Campbell-Brown, 2020). Several models aiming to reproduce the physics involved in the atmospheric entry of a meteoroid have been developed over the last decades. The best review of all such physical process was recently performed by Popova et al. (2019) and Borovička et al. (2019).

The present study, initiated in 2014, was motivated by the start of the FRIPON project (Colas et al., 2020). The goal was to derive a rough picture of the meteorite fragment distribution on the ground, following a fireball observation and the fall of a meteorite. In addition, the full exploitation of the "CABERNET" project data (Atreya et al., 2012) requires the modeling of small meteoroid entry in the atmosphere. Ideally, any meteor observation pipeline would include such modeling to better understand the meteor phenomenon (see e.g. Sansom et al., 2019; Baláž et al., 2020; Vida et al., 2021). An additional motivation of this work was the need to estimate the number of meteorite fragments in the atmosphere at any given time, for aircraft safety and risk evaluations. Such number can also be compared to the number of artificial debris surviving the entry in the atmosphere, for the same purpose. In this scope, a collaboration with CNES (French Space Agency) and IAAS (International Association for the Advancement of Sapce Safety) was conducted. In addition, the AFM tool was applied to planet Mars, in order to infer the number of meteoroid impacts to be expected and later to be compared to the InSight measurements (Daubar et al., 2018); For this, we were inspired by McAuliffe and Christou (2006a). The developed software called

[1]IMCCE, Observatoire de Paris, univ. PSL, CNRS, Sorbonne Université, Univ. Lille, France.
Email: jeremie.vaubaillon@obspm.fr
[2]IMCCE, Observatoire de Paris, univ. PSL, CNRS, Sorbonne Université, Univ. Lille, France.

IMO bibcode WGN-501-vaubaillon-afm
NASA-ADS bibcode 2022JIMO...50...17V

"AFM" (for Ablation & Fragmentation Model) written in Fortran 90 is freely available upon request[a].

Several aspects described in this paper are probably not new to the reader, especially since the model was presented during the International Meteor conference 2015, but never published so far. However, the way the fragmentation is taken into account is original to some aspects. The goal of this paper is to describe the model (section 2), its implementation in a software (section 3) and applications to several cases (small meteoroid, large asteroid entering the Earth or Mars atmosphere etc., see section 4).

2 Model

2.1 Generality

As a meteoroid enters a planet atmosphere in the continuous regime, it inevitably experiences ablation due to its high encounter velocity (a few 10 km.s^{-1}), and may subsequently show fragmentation. Figure 1 shows the classic view of these two phenomena and associated light-curves. In the case of a simplified single body ablation, the meteor light-curve peaks toward the end because of the exponential atmosphere pressure profile. In the case of a fragmentation, the light-curve peaks early because of the sudden high increase in ablation area right after the fragmentation.

As mentioned above, the best review of all the resources to simulate the ablation and fragmentation of meteoroids in the atmosphere was recently performed by Popova et al. (2019). Complementary works from wind tunnel experiments and full simulation of many aspects of atmosphere entry may be found in Ferrier (2012).

2.2 Ablation

The model developed here aims to broadly reproduce these two phenomena in a simplified way. The ablation model giving the mass-loss rate $\frac{dm}{dt}$ for a single body is inspired by McAuliffe and Christou (2006a), Campbell-Brown and Koschny (2004), and Borovička et al. (2007), with the system of equations based on the conservation of energy:

$$\frac{dm}{dt} = -\frac{\Lambda}{2Q} S_m \rho_{air} V_m^3 \tag{1}$$

$$\frac{dV}{dt} = -S_m \Lambda \frac{\rho_{air} V_m^2}{M_m} + \mathscr{G} \cos\alpha \tag{2}$$

$$\frac{dh}{dt} = -V_m \cos\alpha \tag{3}$$

$$\frac{d\alpha}{dt} = -\mathscr{G} \frac{\sin\alpha}{V_m} \tag{4}$$

$$\frac{dl}{dt} = V_m \sin\alpha \tag{5}$$

with:

- Λ the accommodation (or heat transfer) coefficient (= 1 here)
- V_m the particle velocity [m s^{-1}]
- S_m the particle equivalent sectional area [m^2]
- r_m the particle radius [m]
- ρ_m the particle density [kg.m^{-3}]
- Q the latent heat of (heating+vaporizing) phenomena [J kg^{-1}].
- α the zenith angle [deg]
- ρ_{air} the air density [kg.m^{-3}]
- h the altitude of the particle [m]
- l the ground path length [m]
- $\mathscr{G}$ the acceleration of gravity [m.s^{-2}]

Note that Equation 2 might be written in vectorial terms (see Popova et al., 2019). In practice we consider spherical particles by default (unless specified). Equation 2 becomes: $\frac{dV}{dt} = -\frac{3}{8} C_D \frac{\rho_{air}}{\rho_m} \frac{V_m^2}{r_m} + \mathscr{G} \cos\alpha$, with C_D the drag coefficient. The parameter Q was derived by Borovička et al. (2007) for the particular case of the Draconids. They found $Q = 10^7$ J kg^{-1}.

2.3 Fragmentation

The classic picture of the fragmentation is to consider that a meteoroid will fragment when the dynamic pressure is larger than its tensile strength. Such tensile strength depends on the meteoroid size, material, and global structure. The size dependency is modelled as a log-log mass – tensile strength diagram, hereafter referred to as "MP diagram". It is worth mentioning that the asteroid community sometimes model a meteoroid (or asteroid) with a line of constant slope $a = -0.25$ in such a diagram. Inner cracks of local fragility induces by the formation process and subsequent collisions may make the whole picture of a real meteoroid quite complicated.

Popova et al. (2011) clearly showed (see Figure 2) that indeed, a simple linear law (in log space) does not well represent the meteorite falls observed by the meteor community. We have thus chosen to implement the two different approaches, with the following considerations:

F.1 The dynamic pressure P endured by the particle from the atmosphere is computed as $P = \frac{C_D}{2} \rho_{air} V_m^2$, with $C_D = 2$ the drag coefficient of a sphere.

F.2 By default, the model considers a linear law of constant slope in the MP diagram. The relation between the mass and tensile strength is given by $P_{TS} = a * (b/M)^c$, with $a = 10^8$, $b = 2.7\,10^{10}$, $c = 0.25$ (Beech, 2013). In order to allow for some small variations, we consider:

$$P_{TS} = c_p * a * (b/M)^c \tag{6}$$

[a] https://gitlab.com/vaubaill/AFM/

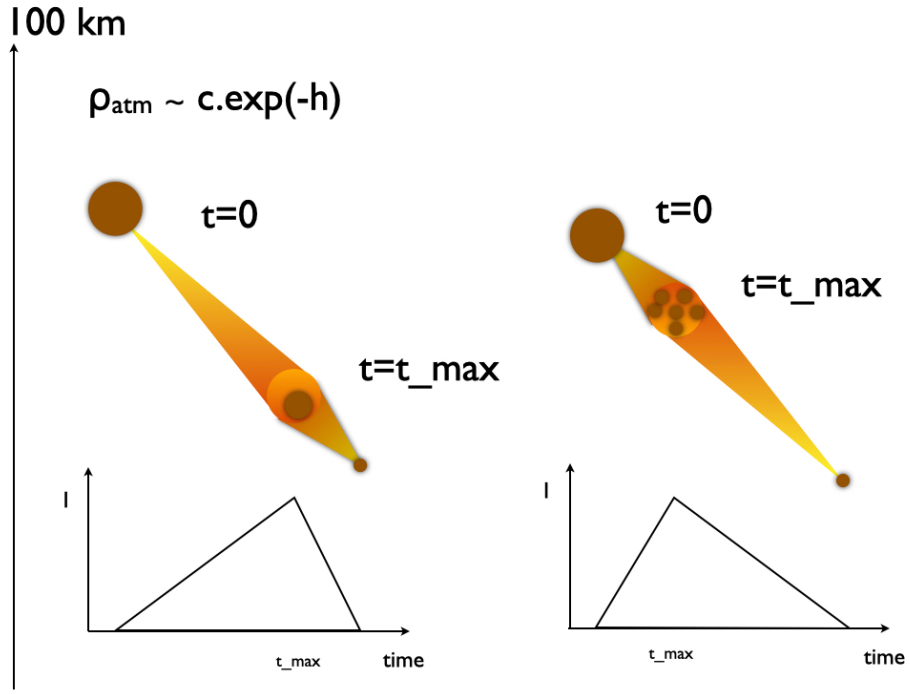

Figure 1 – A simplified view of ablation in the case of a single body (left) and of a fragmentation, and associated meteor light-curve profiles.

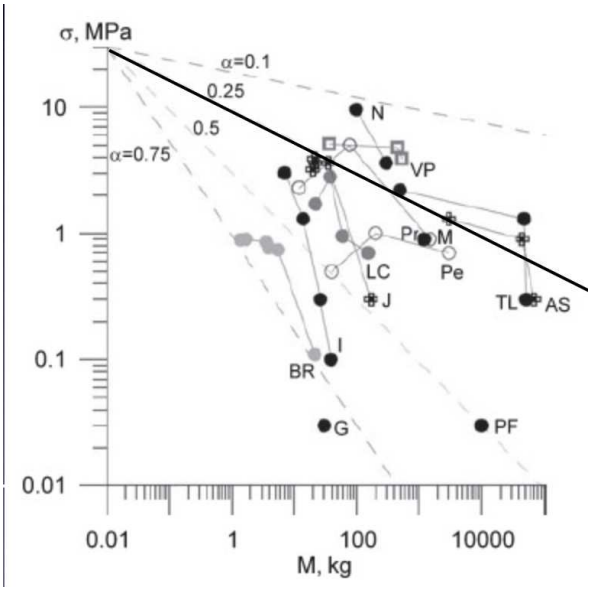

Figure 2 – Mass versus tensile strength (MP) diagram from fireball observations and meteorite recovery, from Popova et al. (2011). Superimposed is the often assumed linear law of constant slope −0.25.

with c_p a coefficient allowing for a distribution around the nominal value ($c_p \in [0.1; 0.9]$). Note that the user may choose different values for the parameters a, b or c.

F.3 However, as shown by Popova et al. (2011), a constant slope in the MP diagram might not correctly reflect the reality. Instead, different methods (meteorite analysis, or fireball observations) allow scientists to measure several data points in the MP diagram. These points better represent a specific meteorite. Therefore, the AFM model takes into account each of the measured [Mass;Pressure] dataset (i.e. points in the MP diagram), and assumes a linear variation from one point to the next. Each tabulated data point is specified by the user in the software configuration file. Note that in order to provide such data, a preliminary estimate of fragments mass is necessary. In the scope of using the present approach in a workflow pipeline, an iterative process must be implemented. This approach allows for a flexible modeling of the meteoroid tensile strength (compared to a constant slope), and presumably a better simulation of the fragmentation stage, for a given fireball.

F.4 If at any stage $P \geq P_{TS}$ then a fragmentation occurs, resulting in N fragments

F.5 The number of fragment N is computed thanks to a given distribution, such as

$$\log_{10} F = \frac{-N}{c_n \times r} \tag{7}$$

where F is the cumulative distribution function, $r \in]0; 1[$ the power index and $c_n \in [0.1; 0.9]$ a coefficient allowing a distribution around the nominal value.

F.6 The mass of each fragment is then computed thanks to a Grady distribution (Vinnikov et al., 2014; Gritsevich et al., 2014), such as $F_m(m > m_0) = 1 - \exp(-\frac{m}{\mu})$, with F_m the cumulative mass distribution function, m the mass of fragment and μ the average mass of all fragments. In practice, random numbers are generated to produce the desired distribution. While such math-

ematical equation may lead to negative value of the mass, we only consider realistic fragments in practice, with the additional constraint of conservation of total mass during the instantaneous fragmentation.

F.7 In order to reproduce the mutual interaction of the fragment, a constant velocity drift might be added. However the physical reasons for such drift are not well understood (Stokan & Campbell-Brown, 2014).

3 Implementation

3.1 Composition and shape

For sake of simplicity, the meteoroids are considered as spherical bodies, which of course might not be realistic, especially for large meteoroids (Popova et al., 2019). The physical data for all possible materials are taken from McAuliffe and Christou (2006a) (see Table 1). In practice, icy meteoroids may only exist beyond the ice line in the current Solar System, which is usually set around 3 AU. Unless someone is interested in simulating icy meteoroids in giant planets or large satellite atmospheres, such composition is not considered here.

3.2 Atmosphere model

One needs to also model the atmosphere profile during the meteoroid hypervelocity entry starting at altitudes of approximately 120 km, i.e. when the density starts to ablate the body and affects its velocity. Several models are available today. The widely used U.S. Standard Atmosphere 1976 (National, 1992) does not provide any data above 86 km of altitude and is therefore not recommended. A simple exponential model does not well reproduce the atmosphere pressure at high altitude either. It appears that interpolation from MSIS-E 90 model is better to be employed (Hedin, 1991). Note that Mars atmosphere data have also been included in the software (Daubar et al., 2018).

3.3 Numerical integration

A "AFM" software is written in Fortran 90 and is freely available upon request[b]. It includes an optional parallelism capabilities thanks to the MPI library.

The numerical integration of the differential equations in Section 2.2 is performed with a Bulirsch & Stoer algorithm with a precision of 10^{-6} and an automated time integration step of initial value of 10^{-3} s. The initial conditions are set by the user and includes: mass, velocity, entry angle, atmosphere model, material, and three possibilities for the fragmentation (none, **F.2** or **F.3**). The default initial altitude is 120 km and the default entry angle is 45 deg.

A test of the fragmentation process is performed at each time step of the ablation process. If a fragmentation occurs, each child meteoroid is integrated individually at the following time step. This means that mutual dynamical interaction between the particles is not considered here. Any child meteoroid might fragment later on. When the slope of the MP diagram (see section 2.3) is close to 0, the fragmentation process happens for nearly any considered mass. This causes a catastrophic fragmentation since all considered sub-fragment will fragment again. A very high number of fragments is generated this way. It is worth mentioning that this holds only for the mass range where the MP slope is close to zero, and given the refinement of the fragmentation model (**F.3**), this might be limited by tabulated data.

The computation of the disintegration of a fragment is stopped whenever its altitude reaches a given target altitude H_{min} (resulting in the storage of the physical conditions), or its mass reaches M_f (after which the particle is considered as completely disintegrated). The value chosen for the H_{min} and M_f depends on the application:

- CNES wanted to know the risk endured by an aircraft from a meteorite fall, and set $H_{min} =$ 16 km and $M_f = 10^{-2}$ kg
- for meteorite density on the ground, we set $H_{min} = 0$ km and $M_f = 10^{-1}$ kg
- for small meteoroid studies, H_{min} does not matter since the whole body will ablate before reaching the ground, and an very low value is set for: $M_f = 10^{-8}$ kg

The program can be run on a single processor or, since it is parallelised, on a supercomputer cluster. The CPU time also varies depending on the initial mass and the fragmentation process, from a few seconds to several hundred hours.

3.4 AFM output

The data produced by the AFM software include the following physical parameters as a function of time, as well as their time derivative: mass, radius, velocity, altitude, zenith angle, horizontal and transverse distances.

In case of a real meteorite fall, such result might help in providing a crude estimate on the fragment distribution to expect on the ground. At the very least, this tool provides indication of the flight of the meteorite after its observation with video cameras. Note that the derivation of the largest final mass must be tuned to the observed data one way or another, which necessitates an additional development (Sansom et al., 2019).

4 Examples of AFM applications and discussions

Ideally, each simulation example provided in this section should be individually and carefully tuned for the desired application, and published separately. In this section, we rather provide a wide overview of the AFM capabilities, and quickly discuss its advantages and limitations.

[b] `https://gitlab.com/vaubaill/AFM/`

Table 1 – Physical properties of the considered materials (from McAuliffe and Christou (2006a)). Water ice is not considered for meteoroids at 1 au.

Name	Units	Rock	Water ice	Iron
Specific Heat	J/kg/K	+9.6E+02	+4.2E+03	+6.9E+02
Density	kg/m^3	+3.4E+03	+1.0E+03	+7.8E+03
Emissivity		+1.0E+00	+1.0E+00	+1.0E+00
Tmelt	K	+1.8E+03	+2.7E+02	+1.8E+03
Latent Heat < Tmelt	J/kg	+8.1E+06	+2.8E+06	+6.5E+06
Latent Heat > Tmelt	J/kg	+6.7E+06	+2.5E+06	+6.4E+06
Mass Unit	kg	+8.3E-26	+3.0E-26	+9.3E-26
Thermal conductivity	W/m/K	+2.0E+00	+1.6E+00	+6.0E+01
Condensation coeff		+0.5E+00	+0.5E+00	+1.0E+00

4.1 Meteorite falls

The Chelyabinsk super-bolide of February 2013 has been widely studied (Borovička et al., 2013; Popova et al., 2013; Brown et al., 2013). The published data provide us insight with the altitude of the light-curve spikes, and the dynamic pressure may be computed assuming its velocity was nearly constant. Assuming moreover a constant slope of 0.165 in the MP diagram leads to a first fragmentation around the observed altitude (around 40 km). The simulated surviving fragments mass follow a Grady distribution because of the underlying assumption (**F.6**, see also Gritsevich et al., 2014). The largest fragment weights $\sim 10^{2.4}$ kg, which is roughly what was recovered ($\sim$ 600 kg). Figure 3 shows the distribution of the fragments at the end of the simulation. The expected total number of fragments is overestimated compared to Borovička et al. (2013), but the model foresee one large fragment accompanied by many smaller ones.

The AFM software does not simulate the extremely complicated interactions between the atmosphere and large meteoroids, nor the complicated physics underlying the fragmentation process. For this, the reader is referred to Popova et al. (2013) and Popova et al. (2019). Similarly, the constant slope in the MP diagram is obviously an oversimplification. However, the order of magnitude of the largest fragment is correctly predicted, as well as the presence of numerous fragments on the ground.

Initial masses of other observed meteorite falls can be found in Popova et al. (2011). By default, the AFM software considers a constant slope in the MP program, and several simulations are first run to estimate the best value that would reproduce the observe light-curve spike. In practice, some cases are extremely hard to model using this way. Trying to reproduce the Grimsby meteorite proved to be extremely difficult; this is the reason why we introduced a way to specifically tune the MP law by allowing the user to specify the data. Figure 2 provides the required MP-diagram data to be taken into account. For the Innisfree meteorite, 7 data points may be specified in the AFM software, and up to 11 for Al Mahatta Sitta. An extensive study of all these meteorites fall would be very interesting and would certainly lead to a revision of the considered model.

4.2 Fakeors

Following McAuliffe and Christou (2006b), the data produced by the AFM sofwtare may be converted into artificial meteors, also known as "Fakeors" (from Barentsen, 2010), in order to simulate its observation from a fixed or moving camera (see e.g. Vaubaillon et al., 2021)[c]. Note that this requires to compute or assume the luminous efficiency τ, which is generally poorly constrained (Drolshagen et al., 2021). In addition, a projection of the data into 3D is required, since the model is 2D only.

Such an approach is computationally more intensive than in Bouquet et al. (2014), but allows the user to take fragmentation into account. The apparent magnitude of each fragment can be computed, and summed up for each pixel of the camera, in order to best simulate the signal received by the sensor. Such simulation requires the knowledge of the whole acquisition chain: lens (ideally with a model of distortion), sensor (number and size of pixels, noise, quantum efficiency etc.).

One tremendous advantage of creating fakeors and simulating their observation with cameras, is to asses the accuracy and precision of a given system, and (most of all) of a trajectory and orbit determination method. Such approach was used by several authors in the past (Gural, 2012; Egal et al., 2017; Vida et al., 2018) and underlined the extreme difficulty to derive an accurate orbit.

The AFM software may be used as well to produce fakeors to compare to real measurements and help to compute the mass of meteoroids (Atreya et al., 2012). For very small meteoroids, the MP diagram might highlight some extreme values and be extended to smaller masses as currently considering in Figure 2.

4.3 Number of meteorite on a planet

The AFM software might be extensively used to estimate the flux of meteoroid at the surface of an atmospheric planet. For this, a synthetic population of large meteoroids (or asteroids) at the top of the atmosphere is needed. Such a population must include the size (or mass) distribution as well as the orbital distribution. The application to Mars was published in Daubar et al. (2018) and Stevanović et al. (2017).

[c] https://academic.oup.com/mnras/advance-article-abstract/doi/10.1093/mnras/stab2727/6375796

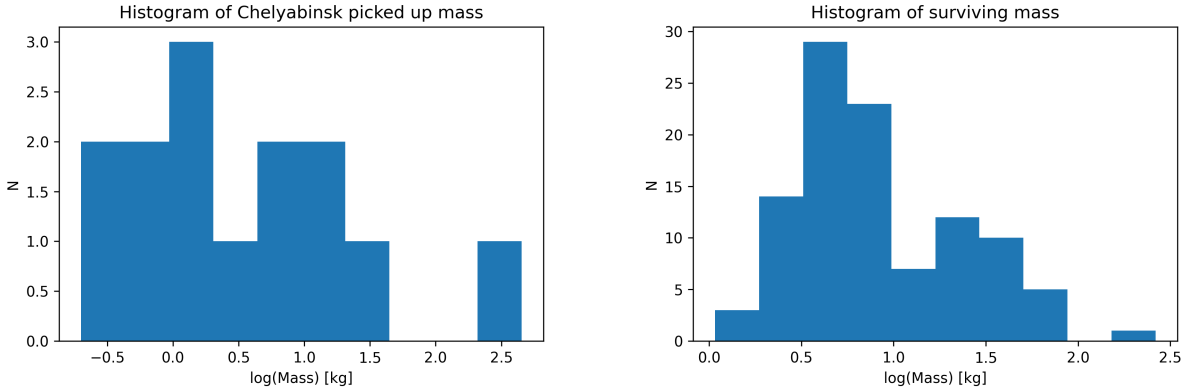

Figure 3 – Simulation of the Chelyabinsk super-bolide: histogram of the expected fragments mass on the ground from the Chelyabinsk super-bolide. Left: from Borovička et al. (2013). Right: at the end of an AFM simulation.

For planet Earth, the first unbiased size frequency distribution, tied to the orbital elements, was performed by Bottke et al. (2002). A more recent estimate was performed by Granvik et al. (2018). In this study, we consider a population of 20 000 objects which represents the unbiased population of near Earth asteroids. The data were provided by M. Granvik, Univ. Helsinki, Finland (personal communication – provided in 2014 – see also Granvik et al. (2018)). These data were then converted into an impact velocity and direction, thanks to the approach defined by Neslusan et al. (1998). Figure 4 shows the distribution of the geocentric velocity. Figure 5 shows the direction in the sky from which the object seem to come from. No privileged directions seem to appear in this plot.

137 initial meteoroids were simulated, out of the 20 000 available near Earth asteroids. A distribution of several parameters was chosen:

D.1 a distribution of $b \in [10^{-3}; 9.0 \times 10^{-2}]$ (see Equation 6)

D.2 $r = 0.6$ and $c_n \in [0.1; 0.9]$ (see Equation 7)

They produced a total of 1.4 million simulated fragments on the ground. The calibration of the output data was performed as follow:

- The histogram of energy of fragment was multiplied by their parent body frequency in Brown et al. (2013) diagram, and divided by the number of simulated parent per energy bin.

- A cumulative histogram of fragment energy is produced in Figure 6.

As a result, the Brown et al. (2013) energy diagram is modified by a depletion of large ($> 10^{-1}$ kt TNT) and small bodies ($< 10^{-8}$ kt TNT), respectively due to fragmentation and ablation. In between, there is an overabundance of medium high-energy particles ($\sim 10^{-2}$ kt TNT). However, a closer look shows that assumptions **D.1** and **D.2** tends to generate an excess of this class of energy. Further studies and considerations are needed to fine tune the final energy distribution.

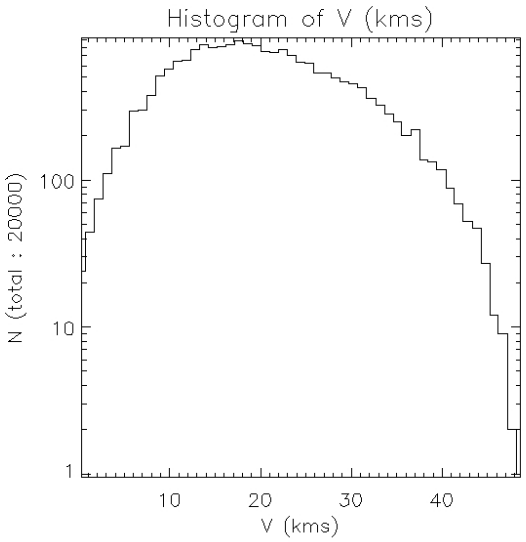

Figure 4 – Histogram of the entry velocity of 20 000 synthetic NEOs, according to a simulation following the unbiased population of Near Earth Objects defined by Bottke et al. (2002).

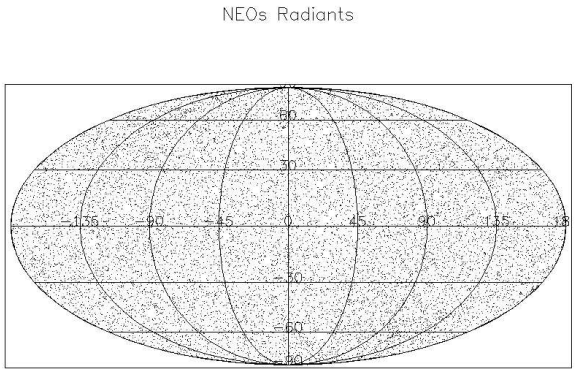

Figure 5 – Radiants (right ascension and declination) from which the (synthetic) near Earth asteroid seem to come from.

5 Conclusion

The AFM software is a simple tool to analyse asteroid/meteoroid atmospheric entry by modeling both their ablation and fragmentation in a planetary atmosphere. It considers a rather simple model in the sense that fancy detailed and thorough consideration of the

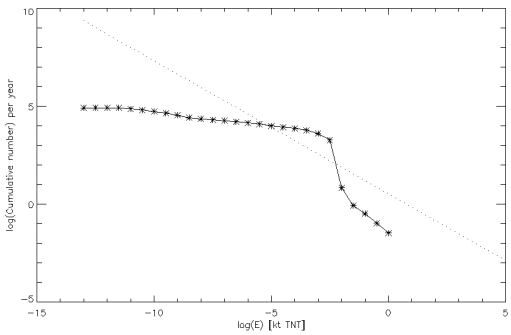

Figure 6 – Calibrated cumulative histogram of the energy at the ground. The doted line is the energy distribution at the top of the atmosphere derived by Brown et al. (2013).

meteor phenomenon are not taken into account. Better models with refined physical modeling can be found in e.g. Popova et al. (2019) and Boslough (2015). However, this tool allows one to quickly estimate the major physical parameters of a meteoroid entry, which is enough to reproduce a meteorite fall, create fakeors (to fine tune an observation setup) and estimate the population of meteorites on a planetary ground or any given altitude. Thorough considerations for each of these applications is needed but would be beyond the scope of this paper, which goal is to provide a global introduction to the AFM software.

Acknowledgements

This work was supported by CNES, the French space agency, under contract n°4700039011. The authors are particularly thankful to Bruno Lazare (CNES/IGQ/T) for his support. The AFM software was run at CINES supercomputer facility.

References

Armitage T. and Campbell-Brown M. (2020). "Constraining the grain mass distribution of small meteoroids using high resolution data". *Planet. Space Sci.*, **186**, 104915.

Atreya P., Vaubaillon J., Colas F., Bouley S., and Gaillard B. (2012). "CCD modification to obtain high-precision orbits of meteoroids". *MNRAS*, **423**, 2840–2844.

Baláž M., Tóth J., Vereš P., and Jedicke R. (2020). "ASMODEUS meteor simulation tool". *Planet. Space Sci.*, **190**, 104937.

Barentsen G. (2010). "Testing trajectory determination algorithms using simulated meteors". In *2010 Meteor Orbit Determination workshop #03, ESA/ESTEC - The Netherlands*.

Beech M. (2013). "Towards an Understanding of the Fall Circumstances of the Hoba Meteorite". *Earth Moon and Planets*, **111**, 15–30.

Bland P. A., Spurný P., Bevan A. W. R., Howard K. T., Towner M. C., Benedix G. K., Greenwood R. C., Shrbený L., Franchi I. A., Deacon G., Borovička J., Ceplecha Z., Vaughan D., and Hough R. M. (2012). "The Australian Desert Fireball Network: a new era for planetary science". *Australian Journal of Earth Sciences*, **59:2**, 177–187.

Borovička J., Spurný P., Brown P., Wiegert P., Kalenda P., Clark D., and Shrbený L. (2013). "The trajectory, structure and origin of the Chelyabinsk asteroidal impactor". *Nature*, **503**, 235–237.

Borovička J., Spurný P., and Koten P. (2007). "Atmospheric deceleration and light curves of Draconid meteors and implications for the structure of cometary dust". *A&A*, **473**, 661–672.

Borovička J., Macke R. J., Campbell-Brown M. D., Levasseur-Regourd A.-C., Rietmeijer F. J. M., and Kohout T. (2019). "Physical and Chemical Properties of Meteoroids". In Ryabova G. O., Asher D. J., and Campbell-Brown M. J., editors, *Meteoroids: Sources of Meteors on Earth and Beyond*, page 37.

Boslough M. (2015). "Airburst Modeling". In *Handbook of Cosmic Hazards and Planetary Defense*, pages 665–692. Joseph N. Pelton and Firooz Allahdadi.

Bottke W. F., Morbidelli A., Jedicke R., Petit J.-M., Levison H. F., Michel P., and Metcalfe T. S. (2002). "Debiased Orbital and Absolute Magnitude Distribution of the Near-Earth Objects". *Icarus*, **156**, 399–433.

Bouquet A., Baratoux D., Vaubaillon J., Gritsevich M. I., Mimoun D., Mousis O., and Bouley S. (2014). "Simulation of the capabilities of an orbiter for monitoring the entry of interplanetary matter into the terrestrial atmosphere". *Planet. Space Sci.*, **103**, 238–249.

Brown P. G., Assink J. D., Astiz L., Blaauw R., Boslough M. B., Borovička J., Brachet N., Brown D., Campbell-Brown M., Ceranna L., and others (2013). "A 500-kiloton airburst over Chelyabinsk and an enhanced hazard from small impactors". *Nature*, **503**, 238–241.

Campbell-Brown M. D., Borovička J., Brown P. G., and Stokan E. (2013). "High-resolution modelling of meteoroid ablation". *A&A*, **557**, A41.

Campbell-Brown M. D. and Koschny D. (2004). "Model of the ablation of faint meteors". *A&A*, **418**, 751–758.

Colas F., Zanda B., Bouley S., Jeanne S., Malgoyre A., Birlan M., Blanpain C., Gattacceca J., Jorda L., Lecubin J., and others (2020). "FRIPON: a worldwide network to track incoming meteoroids". *A&A*, **644**, A53.

Daubar I., Lognonné P., Teanby N. A., Miljkovic K., Stevanović J., Vaubaillon J., Kenda B., Kawamura T., Clinton J., Lucas A., and others (2018).

"Impact-Seismic Investigations of the InSight Mission". *Space Sci. Rev.*, **214:8**, 132.

Drolshagen E., Ott T., Koschny D., Drolshagen G., Vaubaillon J., Colas F., Zanda B., Bouley S., Jeanne S., Malgoyre A., and others (2021). "Luminous efficiency of meteors derived from ablation model after assessment of its range of validity". *A&A*, **652**, A84.

Egal A., Gural P. S., Vaubaillon J., Colas F., and Thuillot W. (2017). "The challenge associated with the robust computation of meteor velocities from video and photographic records". *Icarus*, **294**, 43–57.

Ferrier L. (2012). "Analyse aérothermodynamique de l'entrée atmosphérique d'un géocroiseur à occurence séculaire". *Ph.D. Thesis - ONERA, the French aerospace Agency.*

Granvik M., Morbidelli A., Jedicke R., Bolin B., Bottke W. F., Beshore E., Vokrouhlický D., Nesvorný D., and Michel P. (2018). "Debiased orbit and absolute-magnitude distributions for near-Earth objects". *Icarus*, **312**, 181–207.

Gritsevich M., Vinnikov V., Kohout T., Tóth J., Peltoniemi J., Turchak L., and Virtanen J. (2014). "A comprehensive study of distribution laws for the fragments of Košice meteorite". *M&PS*, **49:3**, 328–345.

Gural P. S. (2012). "A new method of meteor trajectory determination applied to multiple unsynchronized video cameras". *Meteoritics and Planetary Science.*

Hedin A. E. (1991). "Extension of the MSIS thermosphere model into the middle and lower atmosphere". *J. Geophys. Res.*, **96:A2**, 1159–1172.

Jenniskens P., Gural P. S., Dynneson L., Grigsby B. J., Newman K. E., Borden M., Koop M., and Holman D. (2011). "CAMS: Cameras for Allsky Meteor Surveillance to establish minor meteor showers". *Icarus*, **216**, 40–61.

McAuliffe J. P. and Christou A. A. (2006a). "Modelling meteor ablation in the venusian atmosphere". *Icarus*, **180:1**, 8–22.

McAuliffe J. P. and Christou A. A. (2006b). "Modelling meteor ablation in the venusian atmosphere". *Icarus*, **180**, 8–22.

Moreno-Ibáñez M., Gritsevich M., and Trigo-Rodríguez J. M. (2015). "New methodology to determine the terminal height of a fireball". *Icarus*, **250**, 544–552.

National G. D. C. (1992). "U.S. standard atmosphere (1976)". *Planet. Space Sci.*, **40:4**, 553–554.

Neslusan L., Svoren J., and Porubcan V. (1998). "A computer program for calculation of a theoretical meteor-stream radiant". *A&A*, **331**, 411–413.

Pearson K. J., Horne K., and Skidmore W. (2005). "Fireballs, Flares, and Flickering: A Semianalytic, LTE, Explosive Model from Accretion Disks to Supernovae". *ApJ*, **619:2**, 999–1013.

Popova O., Borovička J., and Campbell-Brown M. D. (2019). *Modelling the Entry of Meteoroids*, page 9. Ryabova, Galina O. and Asher, David J. and Campbell-Brown, Margaret J.

Popova O., Borovička J., Hartmann W. K., Spurný P., Gnos E., Nemtchinov I., and Trigo-Rodríguez J. M. (2011). "Very low strengths of interplanetary meteoroids and small asteroids". *M&PS*, **46:10**, 1525–1550.

Popova O. P., Jenniskens P., Emel'yanenko V., Kartashova A., Biryukov E., Khaibrakhmanov S., Shuvalov V., Rybnov Y., Dudorov A., Grokhovsky V. I., and others (2013). "Chelyabinsk Airburst, Damage Assessment, Meteorite Recovery, and Characterization". *Science*, **342:6162**, 1069–1073.

Sansom E. K., Gritsevich M., Devillepoix H. A. R., Jansen-Sturgeon T., Shober P., Bland P. A., Towner M. C., Cupák M., Howie R. M., and Hartig B. A. D. (2019). "Determining Fireball Fates Using the α-β Criterion". *ApJ*, **885:2**, 115.

Segon D., Korlevic K., Andreic Z., Vida D., Novoselnik F., and Skokic I. (2018). "Ten Years of the Croatian Meteor Network". *WGN, Journal of IMO*, **46:3**, 87–95.

SonotaCo (2009). "A meteor shower catalog based on video observations in 2007–2008". *WGN, Journal of IMO*, **37**, 55–62.

Spurný P., Borovička J., and Shrbený L. (2007). "Automation of the Czech part of the European fireball network: equipment, methods and first results". In Valsecchi G. B., Vokrouhlický D., and Milani A., editors, *Near Earth Objects, our Celestial Neighbors: Opportunity and Risk*, volume 236. pages 121–130.

Srba J., Koukal J., Ferus M., Lenža L., Gorková S., Civiš S., Simon J., Csorgei T., Jedlièka M., Korec M., Kaniansky S., Polák J., Spurný M., Brázdil T., Mäsiar J., Zima M., Delinèák P., Popek M., Bahýl V., Piffl R., and Èechmánek M. (2016). "Central European MetEor NeTwork: Current status and future activities". *WGN, Journal of IMO*, **44:3**, 71–77.

Stevanović J., Teanby N. A., Wookey J., Selby N., Daubar I. J., Vaubaillon J., and Garcia R. (2017). "Bolide Airbursts as a Seismic Source for the 2018 Mars InSight Mission". *Space Sci. Rev.*, **211:1-4**, 525–545.

Stokan E. and Campbell-Brown M. D. (2014). "Transverse motion of fragmenting faint meteors observed

with the Canadian Automated Meteor Observatory". *Icarus*, **232**, 1–12.

Vaubaillon J., Rietze A., and Zilkova D. (2021). "MALBEC: fine-tuning of the pointing direction of cameras for stratospheric double-station observation of meteor showers.". *MNRAS*, **508:3**, 3897–3909.

Vida D., Brown P. G., and Campbell-Brown M. (2018). "Modelling the measurement accuracy of pre-atmosphere velocities of meteoroids". *MNRAS*, **479**, 4307–4319.

Vida D., Brown P. G., Campbell-Brown M., Weryk R. J., Stober G., and McCormack J. P. (2021). "High precision meteor observations with the Canadian automated meteor observatory: Data reduction pipeline and application to meteoroid mechanical strength measurements". *Icarus*, **354**, 114097.

Vinnikov V., Gritsevich M., Kuznetsova D., and Turchak L. (2014). "Empirical Fragment Distributions in Meteorites". In *Lunar and Planetary Science Conference*, volume 45 of *Lunar and Planetary Inst. Technical Report*. page 1439.

Wiśniewski M., Żołądek P., Olech A., Tyminski Z., Maciejewski M., Fietkiewicz K., Rudawska R., Gozdalski M., Gawroński M. P., Suchodolski T., Myszkiewicz M., Stolarz M., and Polakowski K. (2017). "Current status of Polish Fireball Network". *Planet. Space Sci.*, **143**, 12–20.

Handling Editor: Javor Kac
This paper has been typeset from a LaTeX file prepared by the authors.

Review of visual meteor observations 2012–2021

Jürgen Rendtel[1]

Visual meteor observations comprise a large amount of data for the study of meteor showers. On average over the past ten years, more than 200 observers submit their data, covering 9 000 to 14 000 hours of effective observing time in 200–280 nights per year and collecting a sample of roughly 50 000 meteors each year. The continuation of this data collection is important to extend existing data series which go back over many decades for some showers. Another important aspect is the establishment of a set of independent observation series and finally the use of different samples to calibrate derived observational data. The IMO's Visual Meteor Data Base also generates semi-automatically ZHR profiles for all showers of the Meteor Shower Working List of the IMO. This paper is an overview over the visual data submitted during the past ten years and demonstrates the ability as well as the limitations of the live graphs provided on the IMO web page. Results discussed in detail include the Quadrantids 2019, the α-Monocerotids 2019, the Orionids 2020 and the Perseids 2018.

Received 2022 February 26

1 Introduction

The appearance of meteors was recorded over centuries, particularly if they occurred in large numbers on a few occasions or as bright fireballs. However, it seems that systematic notes of meteor observations have been taken only from the 19th century onwards. This is certainly connected with the realisation that meteors are of extra-terrestrial origin as first shown for meteorite dropping fireballs by E.F.F. Chladni in 1794 and – among other findings – later confirmed by double-station observations of meteors carried out by students from Göttingen (Benzenberg & Brandes, 1800). Some of the early regular notes about meteor numbers, magnitudes and trail directions have been published in full detail by Heis for the period 1833–1875 (Heis, 1877) or have been collected by others. For example, the compilation of Quetelet (Quetelet, 1841) includes early signs of the Quadrantids as observed by Wartmann. A more detailed description of the early meteor work can be found, e.g., in Kronk (1988).

More than hundred years later, the standardisation of observing and analysing methods during the founding period of the IMO allowed detailed analyses of the activity of meteor showers. Details are described in Koschack et al. (2022).

Reports of observations made before the standards were established do not include the full information of observing conditions and other data necessary for calibration. Nevertheless, we may apply some methods to derive consistent data, such as calibration via the number of non-shower meteors or comparing meteor numbers during a maximum and the period before and/or after this. With some care, we may trace the activity of some well known showers back over decades. Examples are the Orionids (Rendtel, 2008) and the Geminids (Rendtel, 2019). This especially holds for unusual activity, outbursts and meteor storms such as the Leonids (Jenniskens, 2006).

From the 1990-ies onwards, video meteor observations became more and more important as they provide not only counts but also precise orbital data which allow us to deal with the structure of meteoroid streams (Molau & Gural, 2022). Nevertheless, both the visual and video meteor observations complement each other (concerning temporal coverage and establishing an independent sample). Cross calibration during a long overlapping period should guarantee a reasonable transition from the visual data towards the video data. By continuing visual observations we may easily extend the data series for several meteor showers and this way cover their evolution over about 200 years.

Another aspect I personally feel to be important is connected with the appearance of meteors of various brightness and velocity. Independent of the technique used – visual, video, radio, radar – it is of benefit if the observer or analyser has some experience and impression with the way the meteoroids interact with the Earth's atmosphere.

2 Observational data in the current VMDB

2.1 Data collection

The original data base was developed by Roggemans (1988) and further improved and modified by Arlt and Koschack mainly in the 1990-ies, motivated by requirements during the practical use (input of data as well as analysis of shower activity). These programs for the shower analyses allow us to derive reliable data of the rate (ZHR) and population index (r) during the activity periods of essentially all showers in our working list. Of course, the working list has evolved, too. Some showers cannot be found any more, others have been added or had single outbursts only. In order to save storage, the original version used observer codes and site codes. Nowadays, the complete information is stored in one record per session.

2.2 Meteor shower activity graphs

The IMO web page provides ZHR graphs for all meteor showers included in the working list for each return (see `https://www.imo.net/members/imo_live_shower`). These graphs are calculated automatically from the available and incoming data, applying a set of standard parameters which is adapted manually to the

[1]International Meteor Organization, Eschenweg 16, 14476 Potsdam, Germany. Email: `jrendtel@web.de`

IMO bibcode WGN-501-rendtel-visual
NASA-ADS bibcode 2022JIMO...50...26R

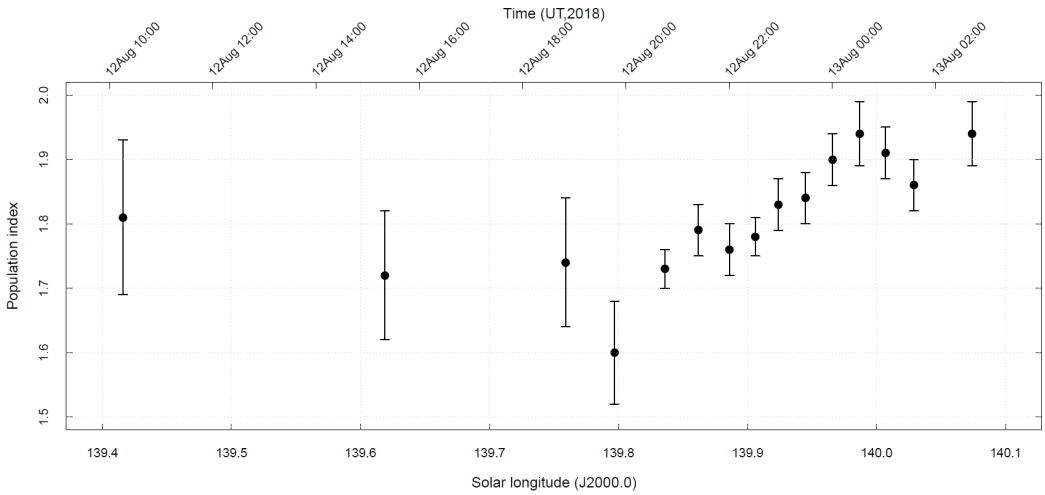

Figure 1 – Analysis of the Perseid meteor magnitudes during the passage through a filament of the stream on 2018 August 12/13.

circumstances of the respective return. This includes the (average) observing conditions of the available reports and the number of reported meteors during the activity period. In most cases, we provide a general ZHR profile for the entire activity period and a separate profile for the maximum of a shower. Especially the population index r is different for the near-peak period and the time off the centre of a shower, hence the graphs cannot represent the appearance of the shower over the entire activity period.

We show just a few examples of major and minor shower activity graphs. Because of the pre-set parameters (r, sample size per bin, minimum limiting magnitude) all these graphs are only meant as an overview of the activity, and cannot replace an analysis of the shower data. This requires an careful analysis of the magnitude data first as described in detail by Koschack et al. (2022), and an adaptive application of the interval data as described for the Perseid 2018 analysis (Rendtel et al., 2019). For comparison, we show the result of the detailed analysis and the automatically generated Perseid graph for the period 2018 August 12, $10^{\rm h}30^{\rm m}$ to August 13, $03^{\rm h}30^{\rm m}$ UT. A major difference is the applied population index. For the live graph, $r = 2.00$ is set for the entire peak period, while the Perseid magnitude data show a change across the cross section through the stream with a distinct minimum of $r = 1.6 \pm 0.08$ at August 12, $19^{\rm h}47^{\rm m}$ UT, shown in Figure 1 (taken from Rendtel et al. (2019)). But also the adaptive selection of data for the ZHR calculation through the maximum period makes a difference. The parameters for the detailed analysis vary during the period, while the ZHR profile shown on the web page has fixed parameters (Figure 2).

Another example for meteor shower rate profiles is the 2019 Quadrantid (010 QUA) maximum shown in Figure 3. For the details see the Figure caption.

Apart from the weather effects, a good data coverage over large geographical regions (continents) depends on the astronomical conditions. The best chances exist for showers like the Geminids or Orionids (see Figure 4) when the respective radiant is well above the horizon for a large fraction of the night. In such cases sessions from observers in neighbouring geographical regions may sufficiently overlap to obtain a continuous profile.

Table 1 – Data of the outburst of the α-Monocerotid on 2019 November 22 for the points shown in Figure 5. The total sample included 228 AMO meteors, and a constant $r = 2.50$ was used for the entire outburst period.
Int. is the number of count intervals for the given average; AMO is the number of shower meteors; ND is the spatial number density in (10^{-9}km^{-3}).

Time (UT)	$\lambda_\odot$ (2000.0)	Int.	AMO	ZHR	ND
04:37	239.°296	14	11	19±6	41
04:42	239.°300	8	11	40±12	86
04:46	239.°303	12	21	38±8	82
04:52	239.°307	15	43	96±1	205
04:57	239.°310	12	42	113±17	243
05:02	239.°314	12	20	60±13	128
05:07	239.°317	13	36	77±13	164
05:11	239.°321	8	17	93±22	200
05:16	239.°324	7	17	48±11	104
05:26	239.°331	9	10	16±5	34

Short periods between radiant rise and twilight, as we find them e.g. for the Eta Aquariids, require lots of intervals from rather small longitude ranges to cover the activity profile, which is essentially not possible.

Independent on all coverage by data obtained by one technique, it is always important to compare and calibrate data from independent data sets. It may help to evaluate the accuracy and reliability of structures found.

Nevertheless, the live graphs on the IMO web page are also meant as a motivation to contribute to the data collection and the immediate information about the activity especially around major shower maxima.

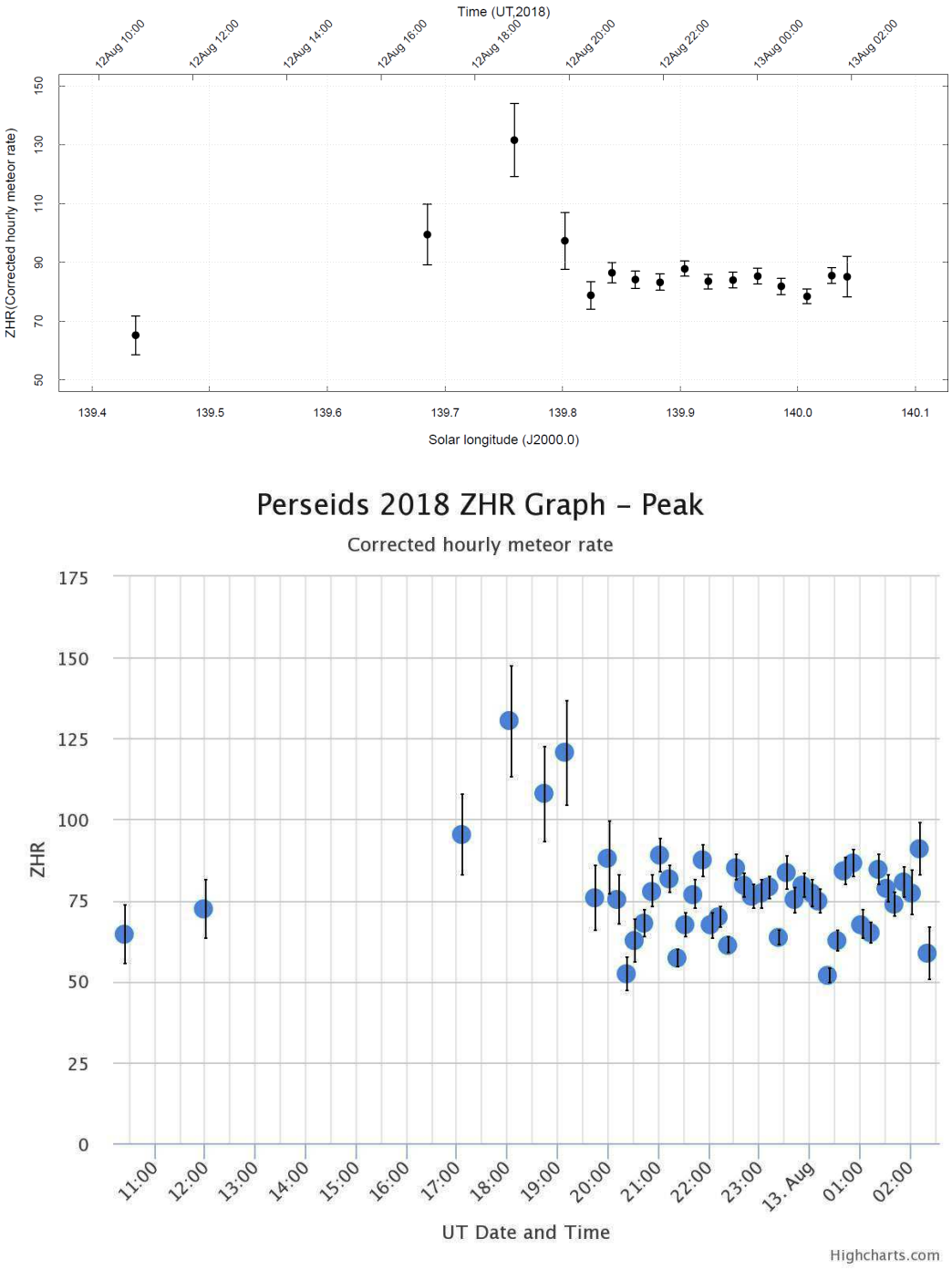

Figure 2 – Comparison of the ZHR profile for the Perseid maximum period in 2018.
Top: result of the adaptive data selection per interval and applying the values of the r-profile shown in Figure 1.
Bottom: the parameters for the shown period are $r = 1.70$, minimum bin length 10 minutes, minimum 50 Perseids per bin, minimum limiting magnitude 5.50 mag.
While the small sample size is fine for the filament crossing time near $19^{\mathrm{h}}10^{\mathrm{m}}$UT, the large number of available reports later would allow to chose a much larger sample and to select data obtained under better conditions (which reduces the bias due to corrections a lot as shown by Koschack et al. (2022)). Then we also obtain valuable data points rather than the cloud of points in the right hand graph which do not tell us anything about the ZHR or flux density.

3 Data in the VMDB 2012–2021

Over many years, Rainer Arlt has developed the programs and maintained the contents of the VMDB and worked as IMO Visual Commission Director. The approval of incoming reports is done by a small group of experienced observers (Rainer Arlt, Bob Lunsford, Ina Rendtel, Jürgen Rendtel). This is mainly to detect more or less obvious errors in the data and to be close to the incoming reports, occasionally contacting an observer to clarify open issues or to get details about data sent for "unknown" radiants, for example. Sometimes observers find out that something was wrong after the submit button was pressed. A short message to Vincent Perlerin will be forwarded to establish contact between the observer (submitter) and the VMDB team to correct the data.

With this brief report I also intend to thank Rainer and the observers for their work. The numbers hope-

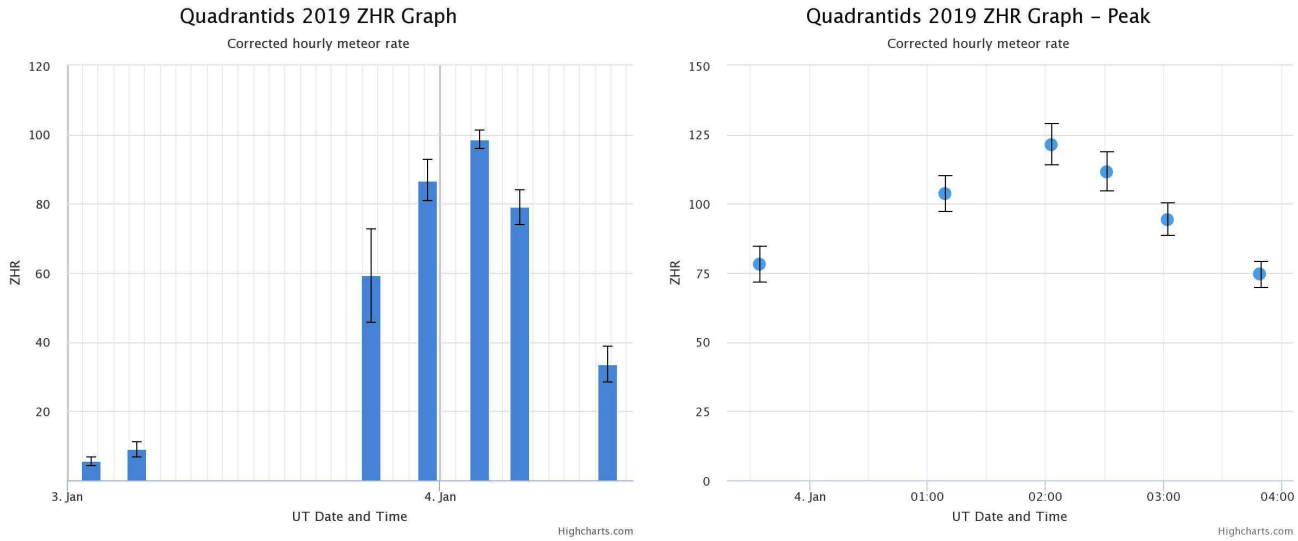

Figure 3 – Visual observations of the Quadrantid activity in 2019.
Parameters for the general ZHR profile (left): $r = 2.50$, minimum bin length 4 hours, minimum 15 Quadrantids per bin, minimum limiting magnitude 5.50 mag.
The peak ZHR profile (right) has another set of parameters: $r = 2.10$, minimum bin length 10 minutes, minimum 250 Quadrantids per bin, minimum limiting magnitude 5.80 mag.
This also implies that the near-peak ZHRs of the general profile are (over-)corrected with a (probably not appropriate and usually higher) population index. Since the 4-hour interval length per bin (left diagram) exceeds the duration of the actual peak, the average "modifies" the true peak ZHR (and perhaps also the position is smeared out).

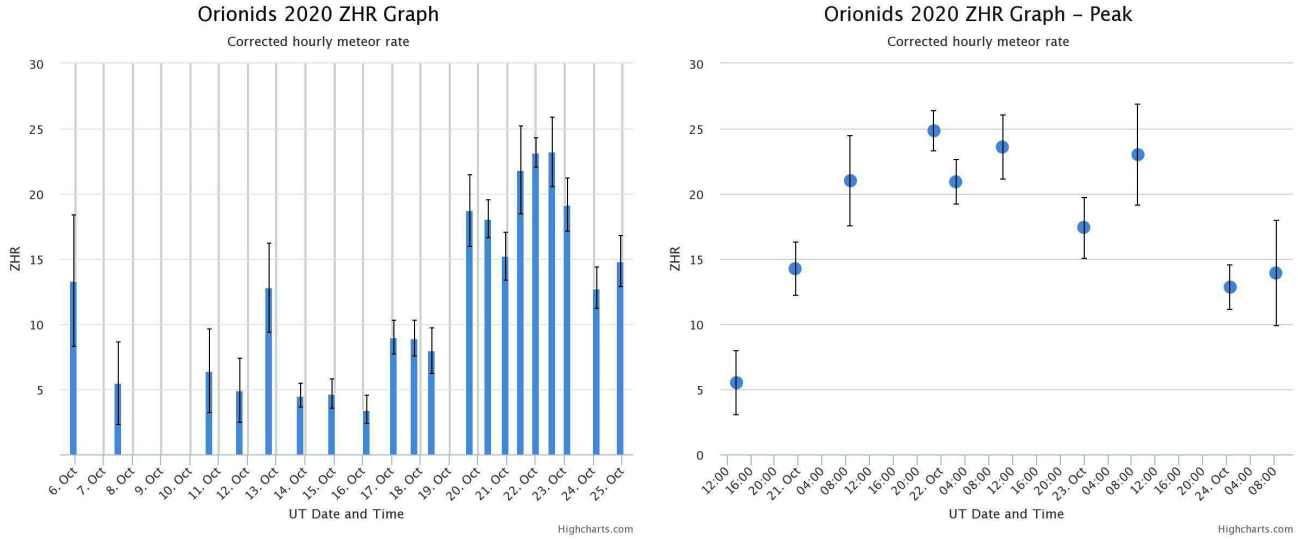

Figure 4 – Visual observations of the Orionid (008 ORI) activity in 2020.
Parameters for the general ZHR profile (left): $r = 2.60$, minimum bin length 12 hours, minimum 40 Orionids per bin, minimum limiting magnitude 5.30 mag (to include intervals closer to the full moon phase and to increase the sample for the periods off the maximum which usually gain less attention).
For the peak ZHR profile (right) another set of parameters was applied: $r = 2.55$, minimum bin length 4 hours, minimum 250 Orionids per bin, minimum limiting magnitude 5.60 mag.
The general profile ends after the maximum due to the interference of moonlight. The maximum graph includes data of reports from various longitude ranges. The rather continuous sequence of data points indicates a good overlap. The largest geographical gaps are due to the Atlantic and Pacific Oceans, respectively (roughly corresponding to 5–8 and 14–19 UT).

fully help to motivate old and new observers to continue with visual observations. This overview covers data collected during the past ten years. It is less than around the major returns of the Perseids in the late 1990-ies until about 2004 and the period of the famous Leonid storms which of course generated a huge interest.

In the subsequent years, the number of reports (and of course the number of meteors) decreased significantly. But the amount of reports we received since 2002 (Table 2) has been on a rather constant level. Variations are to a large extent depending on the moonlight interference with the maxima of the major showers in a given year. (The 2021 numbers may still increase as some reports are submitted with some delay.)

Many observers submit their visual meteor observation data regularly over a long time. Some observers gained experience during more than two decades. Having seen thousands of meteors, it seems that there are

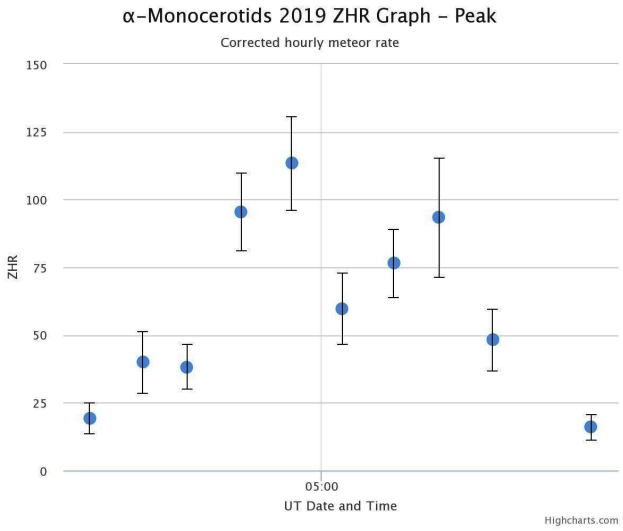

Figure 5 – Activity of the α-Monocerotids (246 AMO) in 2019 in the hour around the short ZHR outburst on November 22. The profile shown in the graph covers only the peak period between 04^h30^m and 05^h30^m UT. Because of the small sample (only 228 AMO meteors), and the attempt to obtain a high temporal resolution of 5 minutes, we reach a point where the results become statistically insignificant (see Table 1) so that any interpretation requires further check of this and independent data sets.

Table 2 – Totals of the visual observing data submitted to the VMDB over the past ten years.

Year	Obs.	Sessions	Nights	T_{eff}	Meteors
2012	486	1814	237	13999	88906
2013	424	1570	211	12519	76006
2014	349	1306	234	9293	44715
2015	456	1516	202	13036	86224
2016	386	1444	215	11626	70486
2017	254	1258	248	9097	43090
2018	302	2002	276	14241	88565
2019	217	1465	281	10927	51169
2020	205	1739	276	13046	60372
2021	192	1521	273	11909	54454

almost no surprises left – which often enough is overridden in the next session. Of course, each contribution is welcome. Nevertheless, we want to add an overview of the most contributing observers during the period 2012–2021 (Table 3).

Below is a list of particular events with enhanced activity or outbursts recorded in these years. Results are also included in the 2019 textbook on meteors and meteoroids, mainly in Chapter 4 (Koten et al., 2019).

- **2011 October 08, October Draconids (009 DRA):** well observed outburst at 20^h09^m UT (video and visual methods (Molau & Barentsen, 2014)).
- **2013 September 09 September ε-Perseids (208 SPE):** increased ZHR (Rendtel et al., 2014).
- **2014 and 2021 – κ-Cygnids (012 KCG):** enhanced ZHR in both years, with numerous bright shower meteors especially in 2021 (Jenniskens, 2021) and a ZHR of the order of 10, about twice the ZHR of a typical return.
- **2014 December 01, Phoenicids (254 PHE):** first activity recorded since the detection of the shower in 1956. ZHR between 20 and 30 observed visually from La Palma (Sato et al., 2014). Another calculated return on **2019 December 02** was confirmed by video observations.
- **2016 July 28, γ-Draconids (184 GDR):** a short outburst with a ZHR of the order of 100 found in video data (Molau et al., 2016), but not observed visually.
- **2016 August 12, Perseids (007 PER):** dust trail encounters between 00^h and 04^h UT (Miskotte & Vandeputte, 2017) with a ZHR of the order of 300 as predicted by several models.
- **2018 October 06, October Camelopardalids (281 OCT):** weak but significant activity (Rendtel, 2018) with a ZHR of the order of 5.
- **2018 October 08/09, October Draconids (009 DRA):** four hours like a major maximum with a ZHR near 150 around 23^h UT and a later, slightly weaker maximum shortly after 01^h UT (Rendtel, 2020b).
- **2018 November, Leonids (013 LEO):** well after the nodal crossing on November 17, several weak dust trail encounters were predicted. The last one was due on November 25. Because of moonlight interference, the amount of data is too small for conclusions. The highest ZHR ≈ 20 is found on November 18, 02^h–03^h UT which does not fit any of the modelled positions and is about 4–5 hours after the nodal crossing.
- **2019 August 31, Aurigids (206 AUR):** enhanced rates observed in the night August 31/ September 01. This weak sign initiated modelling attempts which indicated the possibility of a short activity burst on **2021 August 31** at 21^h17^m UT with a ZHR ≈ 75. Observations confirmed both

Table 3 – Observing time of the most prolific visual observers during the ten year period 2012–2021.

Observer	Eff. observing hours
Jürgen Rendtel, Germany	2093
Terrence Ross, USA	1615
Ina Rendtel, Germany	1111
Adam Marsh, Australia	992
Koen Miskotte, Netherlands	992
Javor Kac, Slovenia	639
Pierre Bader, Germany	505
Michel Vandeputte, Belgium	495
Kai Gaarder, Norway	477
Christoph Gerber, Germany	399

the timing and intensity of the modelled event (Rendtel & Koschack, 2021b).

- **2019 November 22, α-Monocerotids (246 AMO):** predicted and observed outburst (see Figure 5 and the details concerning the data listed in Table 1).
- **2020 November, Leonids (013 LEO):** weak activity was predicted by Mikhail Maslov from some dust trail encounters (see the IMO Meteor Shower Calendar 2020, page 18). Meteoroids of the 1600 trail are leading the comet, like the trails due in the following years – hence the interest in the appearance is of great interest. Unfortunately, the visual data are not sufficient to confirm these although some variations occur close to the expected positions.
- **2021 Aug 14, Perseids (007 PER):** a very late peak about a day after the nodal maximum (Jenniskens & Miskotte, 2021).
- **2021 September/October: Arids (1130 ARD):** meteors of comet 15P/Finlay seen as Arids from far southern locations (Jenniskens et al. 2021) end September (weak) and with a ZHR of about 70 on 2021 October 6/7, caused mainly by meteoroids released from the parent in 2014/15.
- **2021 November 28, Andromedids (018 AND):** a brief outburst close to 05^{h}UT (particularly strong in radar data as communicated to me by Peter Brown) – which was not covered by visual observations but may indicate further events from this source (see Wiegert et al. (2013)).
- **Taurid swarm years in 2012 and 2016**, causing large numbers of bright fireballs in the first days of November (to happen again in November 2022).
- **Geminids (004 GEM):** continuously showed maximum ZHR of about 150 (see, e.g. Rendtel et al. (2020a) for the 2018 return). There is a good coincidence between the modelling of the stream and the observed activity over the past decades (Ryabova & Rendtel, 2018).
- **Ursids:** several filament and dust encounters have been calculated, but the often poor weather at many northern locations did not allow the visual observers to collect sufficient data for an analysis of the events.

4 Prospects for 2022 onwards

The continuation of the observation series is a general goal, keeping in mind the calibration issues and the documentation of the long term activity records described in the Introduction.

The scientific value of visual meteor observations become obvious in the already mentioned long-term studies of shower activity. The well established data are also used as a reference when new flux density data are compared or even reduced to ZHRs (e.g. Egal et al. (2020) and Egal et al. (2022)). To some extent this is similar to the sunspot numbers which are calibrated to the instruments used at the beginning of the observations.

Although the procedures have been applied over more than three decades by now and it seems that all aspects are known or solved, the limiting magnitude correction does not work properly for background illuminated skies (Rendtel & Koschack, 2021a).

Another point where your contributions are welcome is the addition of data you might have from the years before the official start of the VMDB. There is already number of session reports in the VMDB from 1972 to 1988. If you check your (or other's) logbooks and find reports which might be transformed into valid entries for the VMDB, these are welcome. In case you have questions how to handle such probably incomplete reports, do not hesitate to contact me.

As an aside: isn't it a good feeling that you know that others at various locations around the globe continue observing when your session ends or it is not possible for you to collect data for any reason?

For me, it is enjoyable to watch meteors under an unlimited dark sky and to combine many apparently independent data of single meteor strikes in the sky to a comprehensive image of the meteoroid streams and to document their evolution.

Continue your efforts to follow the activity of major as well as of minor showers throughout the year. Each contribution is welcome!

References

Benzenberg J. and Brandes H. (1800). *Versuche, die Entfernung, die Geschwindigkeit und die Bahnen der Sternschnupopen zu bestimmen*. Peters, Hamburg.

Egal A., Brown P. G., Rendtel J., Campbell-Brown M., and Wiegert P. (2020). "Activity of the Eta-Aquariid and Orionid meteor showers". *Astronomy and Astrophysics*, **640**, A58.

Egal A., Brown P. G., Wiegert P., and Kipreos Y. (2022). "An observational synthesis of the Taurid meteor complex". *Monthly Notices Roy. Astron. Soc.*

Heis E. (1877). *Resultate der in den 43 Jahren 1833–1875 angestellten Sternschnuppen-Beobachtungen*. Veröff. der königl. Sternwarte zu Münster, Coln.

Jenniskens P. (2006). *Meteor showers and their parent objects*. Cambridge Univ. Press.

Jenniskens P. (2021). "Enhanced κ-Cygnid (KCG# 0012) activity in 2021". *eMeteorNews*, **6**, 461–462.

Jenniskens P., Cooper T., Baggaley J., Heathcote S., and Lauretta D. (2021). "First detection of the Arid (ARD, # 1130) meteor shower from comet 15P/Finlay". *eMeteorNews*, **6**, 531–533.

Jenniskens P. and Miskotte K. (2021). "Perseid outburst 2021". *eMeteorNews*, **6**, 460–461.

Koschack R., Rendtel J., and Richter J. (2022). "Analyses and calculations". In Rendtel J., editor, *Handbook for meteor observers*. pages 139–173.

Koten P., Rendtel J., Shrbený L., Gural P., Borovička J., and Kozak P. (2019). "Meteors and Meteor Showers as Observed by Optical Techniques". In Ryabova G. O., Asher D. J., and Campbell-Brown M. J., editors, *Meteoroids: Sources of Meteors on Earth and Beyond*, page 90. Cambridge University Press.

Kronk G. (1988). *Meteor Showers*. Enslow Publ.

Miskotte K. and Vandeputte M. (2017). "The magnificent outburst of the 2016 Perseids, the analyses". *eMeteorNews*, **2**, 61–69.

Molau S. and Barentsen G. (2014). "Real-Time Flux Density Measurements of the 2011 Draconid Meteor Outburst". *Earth, Moon and Planets*, **112**, 1–5.

Molau S., Crivello S., Goncalves R., Saraiva C., Stomeo E., and Kac J. (2016). "Results of the IMO Video Meteor Network – July 2016". *WGN, Journal of the IMO*, **44**, 205–210.

Molau S. and Gural P. (2022). "Video observations". In Rendtel J., editor, *Handbook for meteor observers*. pages 91–102.

Quetelet A. (1841). *Nouveau catalogue des principales apparitions d'étoiles filantes*. Nouveaux mémoires de l'Académie Royale Dessciences et belles-lettres de Bruxelles 15, Bruxelles.

Rendtel J. (2008). "The Orionid meteor shower observed over 70 years". *Earth, Moon, and Planets*, **102**, 103–110.

Rendtel J. (2018). "Oktober 2018: Draconiden-Outburst, Camelopardaliden-Aktivität und normale Orioniden". *Meteoros*, **21**, 246–249.

Rendtel J. (2019). "Geminid activity over a century". In Rudawska R., Rendtel J., Powell C., Lunsford R., Verbeeck C., and Knöfel A., editors, *Proceedings IMC 2018, Pezinok-Modra, Slovakia*. pages 114–117.

Rendtel J. (2020a). "Geminids 2018". In Pajer U., Rendtel J., Gyssens M., and Verbeeck C., editors, *Proceedings of the International Meteor Conference*. pages 183–188.

Rendtel J. (2020b). "Minor meteor shower anomalies 2018: predictions and observations". In Pajer U., Rendtel J., Gyssens M., and Verbeeck C., editors, *Proceedings IMC 2019, Bollmannsruh, Germany*. pages 63–68.

Rendtel J. and Koschack R. (2021a). "Calibration of visual meteor observations". *WGN, Journal of the IMO*, **49**, 120–122.

Rendtel J. and Koschack R. (2021b). "Letter – Aurigid outburst on 2021 August 31". *WGN, Journal of the IMO*, **49**, 73–75.

Rendtel J., Lyytinen E., Molau S., and Barentsen G. (2014). "Peculiar activity of the September epsilon-Perseids on 2013 September 9". *WGN, Journal of the IMO*, **42**, 140–147.

Rendtel J., Veljkovic K., Weiland T., Verbeeck C., and Knöfel A. (2019). "Perseids 2018 – analysis of global visual data". *WGN, Journal of the IMO*, **47**, 18–25.

Roggemans P. (1988). "The Visual Meteor Database (VMDB)". *WGN, Journal of the IMO*, **16**, 179–186.

Ryabova G. O. and Rendtel J. (2018). "Increasing Geminid meteor shower activity". *Monthly Notices Roy. Astron. Soc.*, **475:1**, L77–L80.

Sato M., Watanabe J.-i., Tsuchiy C., Moorhead A. V., Moser D. E., Brown P. G., and Cooke W. J. (2014). "Detection of the Phoenicids meteor shower in 2014". *Planetary and Space Science*, **143**, 132–137.

Wiegert P. A., Brown P. G., Weryk R. J., and Wong D. K. (2013). "The return of the Andromedids meteor shower". *Astronomical Journal*, **145:70**, 11pp.

Handling Editor: Javor Kac

This paper has been typeset from a LaTeX file prepared by the author.

Supplement of J14 Meteor Shower Catalog

SonotaCo[1], *S. Uehara, T. Sekiguchi, Y. Fujiwara, K. Maeda, M. Ueda*

Heliocentric orbit parameters of J14 Meteor Shower Catalog are published.

Received 2022 February 21

1 Introduction

This is heliocentric orbit parameters of J14 Meteor Shower Catalog as the supplement of J14 Meteor Shower and Cluster Catalog (SonotaCo et al., 2021), which is requested by IAU MDC meteor shower database registration. The full digital data is on the web page on the references (SonotaCo, 2021).

References

SonotaCo (2021). "PDA / J14: Meteor Shower and Cluster Catalog". `https://sonotaco.jp/doc/PDA/J14` .

SonotaCo, Uehara S., Sekiguchi T., Fujiwara Y., Maeda K., and Ueda M. (2021). "J14: A Meteor Shower and Cluster Catalog". *WGN, Journal of the IMO*, **49:4**, 76–97.

Handling Editor: Javor Kac

[1]SonotaCo Network, Toru Kanamori 2-11-6 Daizawa Setagaya-ku Tokyo 1550032 Japan. Email: `admin@sonotaco.jp`.

IMO bibcode WGN-501-sonotaco-supplement
NASA-ADS bibcode 2022JIMO...50...33S

Table 1 – J14 shower catalog supplement (heliocentric orbit parameters).

iauno	code	a	q	e	peri	node	incl
752	AAC	66.5	0.79	0.99	125.2	17.7	166.9
429	ACB	25.7	0.98	0.96	176.3	308.1	105.2
450	AED	14.1	0.74	0.95	117.1	17.9	122.3
523	AGC	7.7	1.01	0.87	187.4	155.9	74.4
331	AHY	7.5	0.28	0.96	116.8	106.1	56.9
505	AIC	2.1	0.15	0.93	140.4	334.1	17.1
328	ALA	8.3	1.01	0.88	169.4	106.2	95.6
517	ALO	13.1	0.28	0.98	297.0	13.0	112.2
246	AMO	13.0	0.47	0.96	94.3	60.0	133.5
18	AND	2.8	0.81	0.71	236.0	232.2	10.2
466	AOC	18.6	0.69	0.96	69.2	315.1	160.7
1111	AQI	1.8	0.09	0.95	330.3	92.9	41.3
171	ARI	2.4	0.07	0.97	27.8	77.2	27.2
206	AUR	33.4	0.68	0.98	109.5	158.2	148.9
21	AVB	2.5	0.74	0.70	249.1	29.0	6.6
900	BBO	7.9	0.98	0.88	178.6	292.0	82.0
342	BPI	2.3	0.08	0.96	330.8	138.2	24.1
411	CAN	8.9	0.68	0.92	108.1	110.9	111.8
1	CAP	2.4	0.61	0.75	266.5	128.8	7.0
20	COM	16.1	0.56	0.97	262.7	266.1	134.3
388	CTA	5.0	0.07	0.99	331.6	222.9	39.1
497	DAB	26.5	0.68	0.97	111.6	262.9	114.9
334	DAD	2.4	0.98	0.58	177.9	254.9	73.0
994	DBC	1.9	0.10	0.95	148.4	96.0	26.0
885	DEV	14.0	0.96	0.93	160.8	275.0	151.4
824	DEX	9.9	0.78	0.92	55.9	88.0	157.4
498	DMH	6.2	0.93	0.85	29.4	84.1	121.9
563	DOU	17.1	0.51	0.97	269.0	268.9	106.4
502	DRV	11.3	0.78	0.93	125.2	253.1	153.1
221	DSX	1.2	0.15	0.87	214.4	8.8	22.4
1120	DUM	5.2	0.92	0.82	211.9	268.0	45.1
530	ECV	3.5	0.80	0.77	55.1	120.9	156.6
23	EGE	6.5	0.77	0.88	238.3	208.0	169.5
529	EHY	16.1	0.36	0.98	106.3	82.0	142.5
145	ELY	36.7	1.00	0.97	191.2	50.0	75.1
893	EOP	14.5	0.96	0.93	201.4	355.1	168.0
513	EPV	12.3	0.63	0.95	105.6	276.9	149.0
191	ERI	11.4	0.94	0.92	31.9	314.2	132.8
1127	ESL	2.1	0.08	0.96	150.4	148.1	22.2
31	ETA	10.8	0.57	0.95	96.3	45.1	163.6
746	EVE	2.4	0.98	0.59	6.4	73.2	75.5
11	EVI	2.5	0.43	0.83	285.0	356.9	5.4
548	FAQ	2.0	0.13	0.94	324.0	108.9	33.6
1123	FFH	11.0	0.93	0.92	26.3	94.0	125.4
1125	FFL	2.5	0.10	0.96	146.7	138.0	21.5
531	GAQ	12.1	0.99	0.92	195.7	51.0	120.9
4	GEM	1.3	0.15	0.89	324.2	262.0	22.5
139	GLI	2.2	0.39	0.82	290.2	35.9	6.3
404	GUM	2.6	0.95	0.64	204.4	299.0	47.0
1124	HTV	8.1	0.68	0.92	111.3	293.1	145.6
343	HVI	2.9	0.76	0.73	64.6	220.0	0.9
16	HYD	14.8	0.25	0.98	120.1	74.9	128.8
458	JEC	21.6	0.92	0.96	216.5	82.2	95.3
459	JEO	2.4	0.89	0.62	226.6	92.8	4.9
431	JIP	23.4	0.90	0.96	219.9	93.7	112.3
319	JLE	7.4	0.05	0.99	334.6	281.9	105.1
175	JPE	17.3	0.59	0.97	262.0	108.0	148.9
510	JRC	14.0	1.00	0.93	192.2	84.2	88.7
829	JSP	8.2	0.69	0.92	250.9	108.8	158.2
344	JUG	26.8	0.98	0.96	202.8	125.1	40.2
533	JXA	21.0	0.82	0.96	307.2	285.0	172.2
793	KCA	4.7	0.06	0.99	152.3	109.1	31.3
12	KCG	3.2	0.98	0.70	204.5	136.6	33.9
336*	KDR	10.1	0.93	0.91	209.4	250.9	73.5
445	KUM	18.8	0.99	0.95	187.3	222.9	129.5
1121	LAD	—	0.13	1.00	317.6	278.9	73.9
1119	LAV	6.7	0.94	0.86	24.4	79.1	87.2
13	LEO	7.9	0.98	0.88	173.0	236.0	162.2
22	LMI	16.0	0.62	0.96	103.2	207.9	124.8
524	LUM	15.9	0.92	0.94	147.1	214.9	114.6
6	LYR	22.0	0.92	0.96	214.2	32.1	79.5
520	MBC	8.1	0.58	0.93	263.5	54.1	170.2
559	MCB	10.2	0.60	0.94	79.0	58.0	70.2
1118	MLT	17.9	0.57	0.97	261.1	258.9	145.8
19	MON	8.7	0.18	0.98	130.6	77.0	35.7
318	MVE	5.0	0.97	0.80	12.3	84.1	100.0
1117	NEV	12.9	0.51	0.96	271.1	65.9	170.8
1116	NFL	10.2	0.76	0.93	121.0	247.1	156.7
245	NHD	5.4	0.92	0.83	32.0	46.1	138.0
581	NHE	13.5	0.88	0.93	222.2	35.8	65.9
33	NIA	2.0	0.23	0.89	310.3	151.8	2.4
392	NID	3.2	0.99	0.69	174.5	223.0	74.1
250	NOO	12.6	0.12	0.99	139.8	67.9	23.9
215	NPI	2.0	0.34	0.83	297.3	182.1	4.2
488	NSU	53.5	0.82	0.98	229.6	241.0	99.3
17	NTA	2.1	0.38	0.82	292.1	232.0	2.6
337	NUE	7.3	0.92	0.87	36.4	348.0	142.6
1115	NXE	4.3	0.60	0.86	81.7	61.9	19.8
818	OAG	16.7	0.16	0.99	313.4	207.0	128.4
555	OCP	11.1	0.80	0.93	234.4	190.9	85.3
281	OCT	14.7	0.99	0.93	168.8	192.6	77.5
333	OCU	15.8	0.98	0.94	165.3	202.0	101.0
338	OER	3.9	0.53	0.86	90.2	53.0	19.7
569	OHY	6.0	0.66	0.89	73.0	132.1	113.7
514	OMC	16.1	0.53	0.97	88.0	238.0	150.8
873	OMI	14.1	0.57	0.96	83.9	332.9	136.1
13	OML	6.1	0.90	0.85	143.7	221.0	148.4
8	ORI	9.9	0.58	0.94	81.6	27.9	163.8
860	PAN	55.6	0.72	0.99	114.1	72.1	90.3
183	PAU	5.5	0.12	0.98	141.1	315.4	55.7
642	PCE	2.0	0.13	0.93	143.0	338.1	18.3
7	PER	15.5	0.95	0.94	151.0	140.0	113.1
728	PGE	2.3	0.10	0.96	327.5	275.9	18.4
645	PHC	4.2	0.71	0.83	110.6	188.8	161.3
372	PPS	7.1	0.87	0.88	134.5	96.9	150.0
552	PSO	8.8	1.01	0.89	355.6	344.8	135.8
839	PSR	21.2	0.42	0.98	279.7	25.0	69.1
339	PSU	14.9	0.92	0.94	209.4	252.1	117.4
10	QUA	2.6	0.98	0.63	171.9	283.1	70.8
876	ROR	5.0	0.91	0.82	37.5	3.9	144.7
512	RPU	9.1	0.99	0.89	4.2	43.8	105.7
5	SDA	2.5	0.08	0.97	150.2	307.9	26.3
1114	SGC	5.9	0.87	0.85	135.6	202.7	155.0
1113	SJA	13.5	0.87	0.94	314.6	294.9	172.3
526	SLD	3.7	0.98	0.73	190.8	221.9	89.0
1126	SOV	5.8	0.75	0.87	61.0	132.1	161.8
208	SPE	17.5	0.72	0.96	245.9	167.1	139.3
237	SSA	3.8	0.06	0.98	333.5	204.1	23.1
561	SSX	14.1	0.60	0.96	78.1	89.0	151.2
2	STA	2.0	0.36	0.82	113.8	42.9	5.3
480	TCA	5.4	0.85	0.84	132.4	207.0	157.4
535	THC	14.9	0.51	0.97	90.5	312.0	138.0
613	TLY	6.9	0.96	0.86	158.0	198.9	141.7
593	TOL	—	0.70	1.00	245.3	224.2	140.2
340	TPY	15.0	0.96	0.94	20.0	69.0	112.0
571	TSB	74.1	0.49	0.99	270.9	343.0	82.0
543	TTB	4.0	0.94	0.76	154.6	285.1	133.3
507	UAN	9.9	0.70	0.93	110.5	97.1	112.5
1122	UMN	11.4	0.50	0.96	270.8	274.0	101.5
1112	UPI	10.3	0.90	0.91	139.5	107.0	147.5
15	URS	4.9	0.94	0.81	205.8	270.8	52.6
705	UYL	11.9	0.74	0.94	117.0	167.9	115.1
346	XHE	3.5	0.98	0.72	196.7	351.9	60.4
341	XUM	1.5	0.22	0.85	313.6	299.0	67.0
335	XVI	35.4	0.58	0.98	279.7	76.0	170.7
444	ZCS	13.4	0.99	0.93	162.9	114.0	107.4

iauno: IAU numeral code; code: IAU 3 letter code; a: semimajor axis (AU); q: perihelion distance (AU); e: eccentricity; peri: argument of perihelion (J2000); node: longitude of ascending node (J2000); incl: inclination of the orbit (J2000).
* 336 KDR on this paper has been renamed as 336 DKD on current IAU MDC list.

The International Meteor Organization

www.imo.net

Follow us on Facebook InternationalMeteorOrganization

Follow us on Twitter @IMOMeteors

Council

President: Cis Verbeeck,
Bogaertsheide 5, 2560 Kessel, Belgium.
e-mail: cis.verbeeck@gmail.com

Vice-President: Juraj Tóth,
Fac. Math., Phys. & Inf., Comenius Univ.,
Mlynska dolina, 84248 Bratislava, Slovakia.
e-mail: toth@fmph.uniba.sk

Secretary-General: Robert Lunsford,
14884 Quail Valley Way, El Cajon,
CA 92021-2227, USA. tel. +1 619 755 7791
e-mail: lunro.imo.usa@cox.net

Treasurer: Marc Gyssens, Heerbaan 74,
B-2530 Boechout, Belgium.
e-mail: marc.gyssens@uhasselt.be
BIC: GEBABEBB
IBAN: BE30 0014 7327 5911
Bank transfer costs are always at your expense.

Other Council members:
Karl Antier, 16, rue de la République,
F-04100 Manosque, France.
e-mail: karl.antier@gmx.fr
Javor Kac (see details under WGN)
Detlef Koschny, Zeestraat 46,
NL-2211 XH Noordwijkerhout, Netherlands.
e-mail: detlef.koschny@esa.int
Sirko Molau, Abenstalstraße 13b, D-84072
Seysdorf, Germany. e-mail: sirko@molau.de
Francisco Ocaña Gonzalez, C/ Arquitectura, 7.
28005 Madrid, Spain.
e-mail: francisco.ocana.gonzalez@gmail.com
Vincent Perlerin, 16, rue Georges Bernanos,
51100 Reims, France.
e-mail: vperlerin@gmail.com
Jürgen Rendtel, Eschenweg 16, D-14476
Marquardt, Germany. e-mail: jrendtel@aip.de

Commission Directors

Visual Commission: Jürgen Rendtel
Generic e-mail address: visual@imo.net
Electronic visual report form:
http://www.imo.net/visual/report/electronic
Video Commission: Sirko Molau (video@imo.net)
Photographic Commission: Bill Ward
(bill_meteor@yahoo.com)
Generic e-mail address: photo@imo.net
Radio Commission: Chris Steyaert
(radio@imo.net)
Fireballs: Online fireball reports:
http://fireballs.imo.net

Webmaster

Karl Antier, e-mail: webmaster@imo.net

WGN

Editor-in-chief: Javor Kac
Na Ajdov hrib 24, SI-2310 Slovenska Bistrica,
Slovenia. e-mail: wgn@imo.net;
include METEOR in the e-mail subject line

Editorial board: Ž. Andreić, D.J. Asher,
F. Bettonvil, M. Gyssens, C. Hergenrother,
T. Heywood, J.-L. Rault, J. Rendtel,
C. Verbeeck, S. de Vet, D. Vida.

IMO Sales

Available from the Treasurer or the Electronic Shop on the IMO Website	€	$
IMO membership, including subscription to WGN Vol. 50 (2022)		
Surface mail	26	32
Air Mail (outside Europe only)	49	60
Electronic subscription only	21	25
Proceedings of the International Meteor Conference on paper		
1990, 1991, 1993, 1995, 1996, 1999, 2000, 2002, 2003, per year	9	12
2007, 2010, 2011, per year	15	20
2012, 2013, 2014, 2015 per year	25	34
Proceedings of the Meteor Orbit Determination Workshop 2006	15	20
Radio Meteor School Proceedings 2005	15	20
Handbook for Meteor Observers	15	20
Meteor Shower Workbook	12	16
Electronic media		
Meteor Beliefs Project ZIP archive	6	8

2022 March 03 fireball from Slovenia

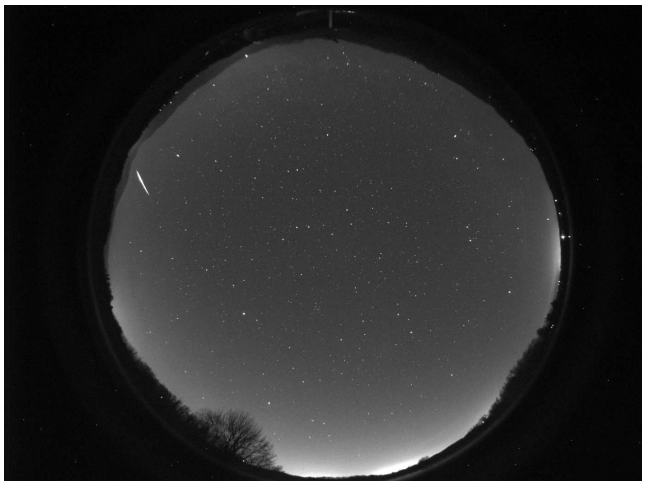

Four views of the same fireball captured from Rezman Observatory, Slovenia on 2022 March 03 at $00^{h}17^{m}16^{s}$ UT. Top: SI0002 camera of the Global Meteor Network; middle: AMS77 camera of the Allsky7 Network; bottom left: CVETKA camera of the IMO Video Meteor Network; bottom right: Rezman Observatory allsky camera.
Images courtesy: Javor Kac, Yves Bastian, Rezman Observatory.